Plasmonics for Laser Beam Shaping

Nanfang Yu, *Member, IEEE*, Romain Blanchard, *Student Member, IEEE*, Jonathan Fan, Qi Jie Wang, Christian Pflügl, Laurent Diehl, Tadataka Edamura, Shinichi Furuta, Masamichi Yamanishi, *Life Fellow, IEEE*, Hirofumi Kan, and Federico Capasso, *Fellow, IEEE*

(Invited Review)

***Abstract*—This paper reviews our recent work on laser beam shaping using plasmonics. We demonstrated that by integrating properly designed plasmonic structures onto the facet of semiconductor lasers, their divergence angle can be dramatically reduced by more than one orders of magnitude, down to a few degrees. A plasmonic collimator consisting of a slit aperture and an adjacent 1-D grating can collimate laser light in the laser polarization direction; a collimator consisting of a rectangular aperture and a concentric ring grating can reduce the beam divergence both perpendicular and parallel to the laser polarization direction, thus achieving collimation in the plane perpendicular to the laser beam. The devices integrated with plasmonic collimators preserve good room-temperature performance with output power comparable to that of the original unpatterned lasers. A collimator design for one wavelength can be scaled to adapt to other wavelengths ranging from the visible to the far-IR regimes. Plasmonic collimation offers a compact and integrated solution to the problem of laser beam collimation and may have a large impact on applications such as free-space optical communication, pointing, and light detection and ranging. This paper opens up major opportunities in wavefront engineering using plasmonic structures.**

***Index Terms*—Laser beams, plasmons, quantum-well lasers, semiconductor lasers.**

I. Introduction

SEMICONDUCTOR lasers are the key components in many widespread commercial technologies such as optical fiber communications and compact disk/digital video disk players. They are also accelerating the development of many other technological fields, including 3-D display technology, quantum information, and medical imaging. However, the output beams of semiconductor lasers have their own problems. First, the beams usually have a large divergence angle of around tens of degrees due to large diffraction caused by the small emission aperture of the devices [1]. Second, light output of semiconductor lasers is mostly linearly polarized along a single direction, which is determined by the optical selection rules of the gain medium [2], [3]. Applications will benefit from the availability of a wide range of polarization states: linear polarization along different directions, circular polarizations (clockwise and counterclockwise), etc.

Laser beam shaping (i.e., collimation, polarization control) is conventionally conducted externally using optical components such as lenses, beam-splitting polarizers, and wave plates [2]. These optical components are bulky and can be expensive; some are available only for certain wavelength ranges.

Devices that have the desired beam characteristics intrinsically built in to the active devices themselves have been designed. For example, devices with an increased effective emission area have been fabricated to reduce beam divergence. Tapered laser waveguides have been used to reduce lateral beam divergence of ridge-waveguide semiconductor lasers [4], [5]. It is not practical to suppress the divergence perpendicular to the material layers by simply growing thick laser active cores; such devices would require unrealistically high voltages for operation and would have heat dissipation problems. Vertical-cavity surface-emitting lasers (VCSELs) [6] have a much larger emission area compared to edge-emitting lasers; correspondingly, they have smaller beam divergence, typically around 10°. This is not enough in situations where ultranarrow divergence of below 1° is needed. In other schemes, to further reduce beam divergence, lasers were processed into surface-emitting structures: 1-D integrated grating outcouplers have helped to create highly directional diode lasers [7]–[22], mid-IR quantum cascade lasers (QCLs) [23]–[27], and terahertz (THz) QCLs [28], [29] with greatly reduced beam divergence in a single dimension. Surface-emitting ring or disk QCLs with 2-D second-order gratings have demonstrated promising results of collimation in two dimensions, but they are complex to design and fabricate and are still in their initial stage of development [30], [31]. In recent years, optically or electrically pumped surface-emitting lasers with 2-D photonic-crystal cavities have been actively investigated [32]–[39]. Two types of structures based on photonic bandgap mode (microcavity) and photonic band-edge mode (distributed feedback) have been demonstrated to achieve controllable far-field emission patterns. In addition to surface-emitting devices, 1-D and 2-D phase-locked diode laser arrays have been created, which exhibit not only reduced beam divergence but also significantly enhanced power output [11]–[13], [16], [17], [40]–[42]. However, phase-locked laser arrays are particularly complicated in design and fabrication.

Manuscript received February 19, 2009; revised June 28, 2009. First published August 11, 2009; current version published January 8, 2010. This work was supported by the Air Force Office of Scientific Research (Multidisciplinary Research Initiative on Plasmonics) and the Harvard Nanoscale Science and Engineering Center. The review of this paper was arranged by Editor E. Towe.

N. Yu, R. Blanchard, J. Fan, Q. J. Wang, C. Pflügl, L. Diehl, and F. Capasso are with the School of Engineering and Applied Sciences, Harvard University, Cambridge, MA 02138 USA (e-mail: nyu@fas.harvard.edu; blanchar@seas.harvard.edu; jfan@fas.harvard.edu; qijie@deas.harvard.edu; pflugl@seas.harvard.edu; ldiehl@seas.harvard.edu; capasso@seas.harvard.edu).

T. Edamura, S. Furuta, M. Yamanishi, and H. Kan are with the Central Research Laboratory, Hamamatsu Photonics K.K., Hamamatsu 434-8601, Japan (e-mail: edamura@crl.hpk.co.jp; masamiya@crl.hpk.co.jp; kan@crl.hpk.co.jp).

Color versions of one or more of the figures in this paper are available online at http://ieeexplore.ieee.org.

Digital Object Identifier 10.1109/TNANO.2009.2029099

In addition to narrow collimation, many devices would benefit from polarization control intrinsically built into the light sources themselves. However, this is very challenging to achieve; for example, the realization of circularly polarized lasers or LEDs has proven elusive [43]–[46].

To summarize, it is difficult or cumbersome to make compact lasers with specific beam characteristics using conventional means. It would be technologically important and very interesting from a scientific point of view to devise a new scheme to provide a compact and universal solution to the problem of laser beam shaping; plasmonics is a very good candidate for addressing these needs.

Plasmonics involves manipulation of surface plasmons (SPs), which are collective surface oscillations of electrons in metal interacting with an electromagnetic field [47], [48]. In contrast to conventional optical components, where amplitude and phase shaping of light are in three dimensions, i.e., along both the light propagation direction and in the plane normal to light propagation, plasmonic structures provide compact and integrated optical processing, where planar metallic structures can be used to manipulate the amplitude and phase of SPs in two dimensions. Furthermore, unlike conventional optical components, plasmonic structures manipulate light at the subwavelength level in real space or over a wide range of k in wave vector space. By integrating plasmonic structures on active optical devices, one can engineer and fabricate devices with small footprints and specific beam profiles in the near-field or far-field. Specifically, one can envision collimators and polarizers constituted of metallic gratings, apertures, antennas, or other configurations. We can go further and ask more challenging questions: is it possible to use plasmonics to realize laser beam steering [9], [12], [41], [49]–[52]? Can we use plasmonics to create special beams such as Bessel beams [53]–[56], which are diffraction-free, beams that are radially or azimuthally polarized [57]–[61], or beams with orbital angular momentum [62]–[65], which can be used to rotate small particles [66], [67]?

There have been a number of demonstrations of functional devices with integrated plasmonic structures. Plasmonic laser antennas defined on laser facets have been created to concentrate laser output light into deep subwavelength regions with high optical intensity for near-IR laser diodes and mid-IR QCLs [68]–[70]. They have potential applications in optical data storage, optical trapping, and near-field optical microscopy or spectroscopy. Metallic gratings or nanorod arrays have been used to select the polarization of the output of VCSELs [71]–[77]. Guo and coauthors used an aperture–groove structure, based on Lezec *et al.*'s work on plasmonic collimation [78], to reduce the divergence angle of VCSELs by about a factor of 2 [79]. It has been demonstrated that directional emission can be produced by patterning 2-D metallic photonic crystals on the facet of LEDs [80]–[82].

Recently, our group demonstrated very small beam divergence in the laser polarization direction in $\lambda_o = 9.9\ \mu\mathrm{m}$ QCLs by patterning a 1-D plasmonic grating on the device facet [83]. We then extended the idea to achieve complete collimation in the laser emission plane using 2-D plasmonic structures [84], [85]. It was shown in both situations that the beam divergence angles were greatly reduced, from tens of degrees for the original devices to just a few degrees for the devices integrated with plasmonic collimators. The fabricated devices preserve good room-temperature performances; the devices with an optimized design exhibit an output power that is comparable to that of the original unpatterned lasers.

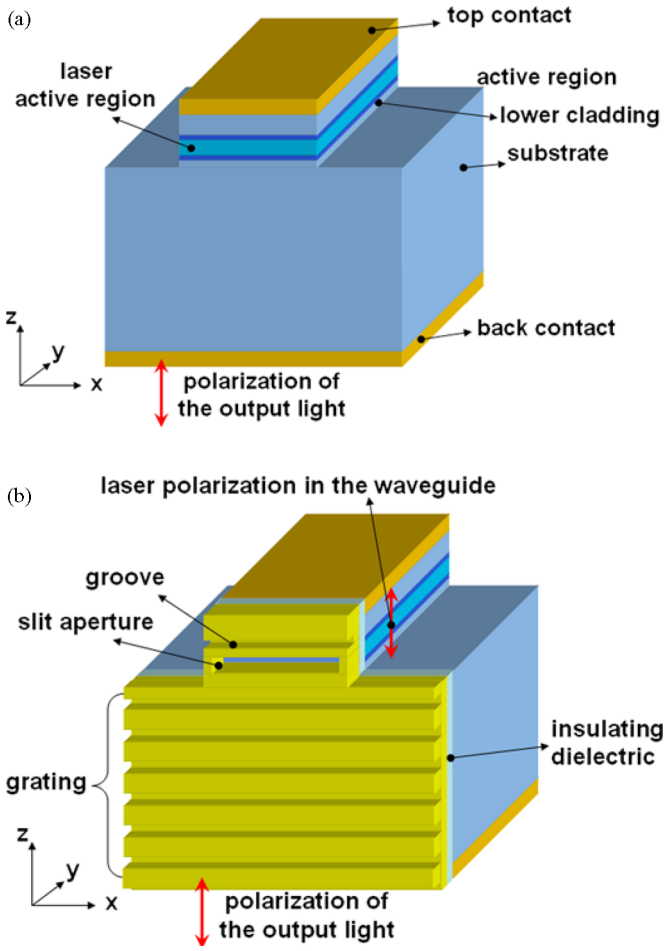

Fig. 1. (a) Schematic of the ridge-waveguide QCL. (b) Schematic of the small divergence laser. It is composed of a QCL and a metallic slit–grating structure defined on its facet.

This paper provides a detailed account of our recent research on 1-D and 2-D plasmonic collimation for QCLs. We choose QCLs as a model system, but the design with proper adjustment should be applicable to diode lasers as well. QCLs are based on transitions between quantized electronic levels confined in the conduction band of a semiconductor heterostructure [86]. As such, QCLs are intrinsically TM-polarized [3]: the electric field is aligned along the growth direction of the heterostructure [z-direction in Fig. 1(a)], which is different from conventional diode lasers where the laser polarization is in the plane of the heterostructure.

This paper is organized as follows. In Section II, we discuss design issues and report experimental results of 1-D collimation. Special emphasis is placed on the physical considerations used to choose the design parameters. In Section III, the design and experimental results for 2-D collimation are reported. Some

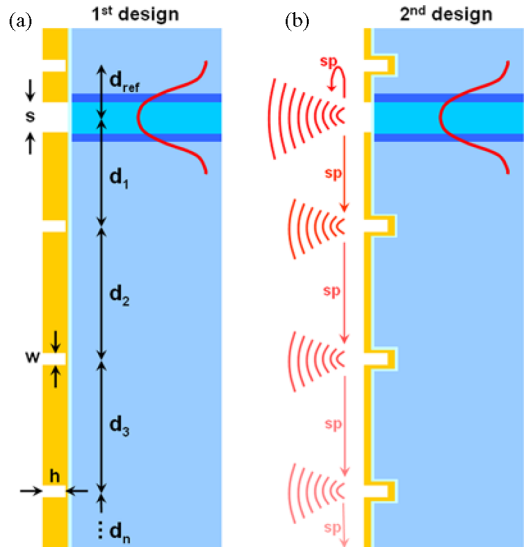

Fig. 2. Cross sections of the two device designs. (a) Slit and the grooves are defined in a thick metal film on the laser facet. (b) Grooves are sculpted into the laser facet and a thin layer of metal is added to cover the patterned facet. There is a dielectric layer between the laser facet and the metal film in both designs for electrical insulation. Only the grooves near the slits are shown in the figures.

specific design considerations arise here, and we will discuss them in detail. Sections IV and V discuss future directions and summarizes the paper.

II. 1-D Collimation

A. Design

The plasmonic collimator works by transferring laser emission into SPs over a large area on the device facet and using grating couplers to scatter their energy into the far-field, thereby breaking the diffraction limit set by the small emission area of the original laser.

The 1-D plasmonic collimator consists of a slit aperture and a grating patterned on the metal-coated laser facet [Fig. 1(b)]. The structure is based on experimental and theoretical works on the beaming of optical and microwave radiation by aperture–groove structures [78], [87]–[94]. The slit aperture and the grating grooves are oriented perpendicular to the laser polarization. The aperture is located on the active region; it is subwavelength in one dimension and covers the entire width of the laser waveguide (tens of micrometers) in the other dimension. Part of the laser output is coupled into SPs by the long edges of the aperture slit. The SPs propagate through the grating along the z-direction and are scattered by the grooves as outgoing radiation (Fig. 2). The separation between the aperture and the first groove [d_1 in Fig. 2(a)] and that between neighboring grating grooves [d_2 to d_n in Fig. 2(a)] are chosen to ensure that the direct emission from the aperture and all the scattered light from the grating grooves are in phase, i.e., the phase difference is equal to integral multiples of 2π. The beam divergence is therefore reduced in the direction normal to the facet due to constructive interference between radiation from the aperture and the grooves. Basically, the beam divergence angle of our devices should be inversely proportional to the number of the grating grooves; in the normal direction, the intensity should scale as the number of grooves is squared (for negligible SP losses): the intensity falls off rapidly with angle θ away from the normal due to the phase factors $\exp(2i\pi nd\ \sin\ \theta/\lambda_{\mathrm{SP}})$ of the waves scattered by the grooves, where n indicates the nth groove, λ_{SP} is the SP wavelength, and d is the grating period designed to be close to λ_{SP}. In summary, the aperture and the grooves in the plasmonic collimator act effectively as an array of coherent light sources, in analogy with phased-array antennas [95]. The latter have been widely used to enhance the directivity of antennas for applications such as directional broadcasting and space communications. In fact, we can use as a figure of merit the concept of antenna directivity for the performance of the plasmonic collimator [96]. The directivity is used here to characterize collimation in the vertical direction, and is defined as $D = 10\ \log_{10}(2\pi I_{\mathrm{peak}}/I_{\mathrm{total}})$, where I_{peak} is the far-field peak intensity and I_{total} is the total intensity under the vertical beam profile. Since mid-IR SPs are capable of propagating over long distances of at least a few hundreds of micrometers [97], tens of grating grooves can be used to couple almost all the energy of the SPs back into free space. The power throughput of the device can therefore be preserved while simultaneously reducing the divergence angle.

The two designs shown in Fig. 2 are effectively equivalent in terms of beam collimation and power throughput, provided that the thicknesses of gold in the collimator are much greater than the skin depth of gold at the lasing wavelength. In the first design [Fig. 2(a)], the coating on the laser facet consists of an insulating alumina film that is a couple of hundred nanometers thick and a gold film thicker than the depth of the grooves. The aperture and grooves are defined in the thick gold film. The second design [Fig. 2(b)] consists of grooves that are sculpted directly into the bare laser facet first, followed by the deposition of the insulating and metallic layers and then the opening of the aperture. The second design is advantageous compared with the first one because it is economical in material usage: the gold film in the second design only needs to be thicker than a few times of the skin depth of gold at mid-IR wavelengths (e.g., about 120 nm for $\lambda_o = 9.9\ \mu\mathrm{m}$) to prevent SPs from penetrating through the metal film. In addition, grooves defined in the semiconductor experimentally show smaller roughness compared to those sculpted into the metal, which helps avoid parasitic scattering of the SPs. On the contrary, the thickness of gold in the first design scales with the lasing wavelength itself, which will be elucidated later in this section, and may be impractically thick.

We note that SPs are generated only on the device facet, i.e., at gold/air interface, not at the inner gold/substrate interface. The latter is a three-layered structure consisting of gold/alumina/InP substrate. This configuration actually does not support low-loss SP modes. To understand this, one should note that in the dispersion diagram the dispersion curve of the SP modes at the gold/alumina interface lies above the light line of InP in the mid-infrared wavelength range since InP has a larger refractive index compared with alumina at the laser wavelength. Therefore, SP modes supported by the gold/alumina interface will quickly lose energy into the InP substrate and will be highly lossy.

In order to yield a small divergence angle, high optical power throughput, and small optical background, several geometric

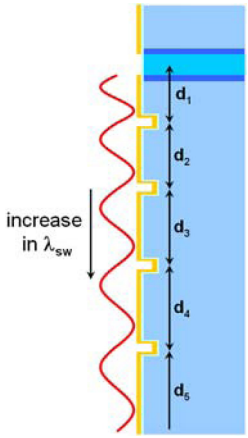

Fig. 3. Schematic showing the evolution of the wavelength of surface waves $\lambda_{\rm sw}$ near the aperture. The change in $\lambda_{\rm sw}$ is due to contributions from SPs and lossy surface waves, which have different wave vectors.

parameters of the collimator need to be optimized, including the vertical width of the slit aperture s, the distance between the first groove and the slit aperture d_1, the distance between neighboring grooves d_2–d_n, the distance between the slit aperture and the "reflector" groove on the top cladding side of the laser facet $d_{\rm ref}$, and the width w and depth h of each groove [Fig. 2(a)]. The following sections discuss physical considerations for choosing these parameters.

1) Width of the Slit Aperture: The vertical width of the slit s needs to be at subwavelength level to efficiently couple radiation from the laser into the SP modes of the grating structure. The optimized value of s is found to be close to the active region thickness ($\sim$2 μm for the $\lambda_o = 9.9$ μm QCLs) according to simulations. A narrower slit strongly backscatters the incoming light, and therefore, reduces power throughput, while a wider slit does not efficiently couple incoming light into the SPs, leading to a large background.

2) Grating Period: The distances d_i should be adjusted to give the correct phase relations for the beams originating from the aperture and from the grating grooves, thus achieving maximum constructive interference between them. Choosing d_i equal to the SP wavelength $\lambda_{\rm SP}$ is not optimal due to the complex form of surface waves generated by the slit aperture. Complete understanding of surface waves generated by a metallic aperture has not yet been achieved [98]–[100], but it has been found that the surface waves exhibit a gradual increase of wavelength $\lambda_{\rm sw}$: $\lambda_{\rm sw}$ is smaller closer to the aperture and progressively approaches a constant as the distance from the aperture increases (Fig. 3). $\lambda_{\rm sw}$ in the immediate vicinity of the aperture could be approximately 5% smaller and the transition range could extend to a distance of about ten times the free-space wavelength [98], [100]. This is basically a diffractive effect: due to the sharp edge of the aperture, the diffracted waves acquire a larger transverse wave vector component closer to the aperture. Considering this effect, an ideal design should have grooves positioned at d_i to match the evolution of $\lambda_{\rm sw}$ so that the phase accumulated by the surface waves in each segment d_i is equal to 2π. Practically, the ideal structure is difficult to design: first, the evolution of $\lambda_{\rm sw}$ is not easy to predict; second, the interaction between the grating grooves and the surface waves will modify the phase relations to some extent, which complicates the problem. As a first-order approximation of the ideal structure, we choose a design with $d_1 < d_2 = d_3 = \cdots = d_n = \Lambda$, and determine d_1 and Λ in simulations by maximizing the peak intensity of the collimated beam. Here, we assume that maximum constructive interference is correlated with maximum collimated optical power. The optimized parameters were found to be $d_1 = 7.3$ μm and $\Lambda = 8.9$ μm for $\lambda_o = 9.9$ μm QCLs.

The fact that $\Lambda = 8.9$ μm is less than $\lambda_{\rm SP} = 9.9$ μm is due to the modification to the SP dispersion curve introduced by the 1-D grating: optical bandgaps are opened in the SP dispersion curve due to the grating [101]. Setting $\Lambda = \lambda_{\rm SP}$ would lead to an inefficient structure because such a grating corresponds to a point in the bandgap, and therefore, prohibits the propagation of SPs. Instead, a $\Lambda = 8.9$ μm grating will modify the SP dispersion curve so that the upper edge of the bandgap is at the laser frequency.

3) Distance Between Aperture and the Top Groove: Due to the limited area of the laser facet, the grating can only be defined on the substrate side of the slit aperture. However, one or more additional grooves can still be included on the other side of the slit, between the slit and the top electrical contact (Fig. 2). Physically, these additional grooves function as a reflector for the SPs propagating toward the laser top contact, thereby reducing scattering at the gold top contact and maximizing the effectiveness of the grating. These additional grooves increase the intensity of the central lobe and reduce the background light. The parameter $d_{\rm ref}$ in Fig. 2(a) is chosen to maximize the constructive inference between the reflected surface waves and the surface waves generated at the aperture and propagating toward the grating.

4) Width and Depth of Grooves: We choose narrow grooves so that each individual groove introduces a small disturbance to the propagation of SPs. We found in simulations that wide grooves comparable to $\lambda_{\rm SP}$ usually provided too strong scattering, and therefore, limited the propagation of SPs to the first few grooves. This would result in limited collimation because narrow collimation requires the scattering of the SPs from many grooves over a very wide area.

The groove depth h is chosen so that cavity resonance condition is satisfied [87], [98]. This makes the otherwise inefficient scatterers, i.e., narrow grooves, effective in coupling the energy of SPs into free space. Note that the groove cavity resonance slightly modifies the phase of the light scattered by the grooves [87], [98], so that d_1 and Λ are adjusted to ensure maximum constructive interference.

Depending on the number of grating grooves N envisioned for a certain design, the groove width and depth, w and h, need to be fine-tuned to ensure that the length of the grating is about two to three times the SP propagation distance (i.e., 1/e decay distance of the electric field $|E|$ of the SPs [97]). This will lead to a structure that scatters almost all the energy of the SPs into the far-field. In this respect, a design with a larger N should have grooves slightly narrower than a design with a smaller N, or it should have groove depth slightly tuned away from the cavity resonance condition to reduce scattering at each individual groove.

B. Simulations

We performed systematic 2-D simulations using the finite-element method (COMSOL Multiphysics) to help design a structure with optimal beam collimation characteristics. The optimized parameters and the complex index of refraction of different materials for $\lambda_o = 9.9\ \mu\mathrm{m}$ QCLs are given in Fig. 4.

We simulated a passive structure (no gain for the laser active region) with a small section (tens of micrometers) of the laser waveguide adjacent to the laser facet. In the simulations, we first solved a boundary eigenmode problem to obtain the fundamental TM_{00} mode of the laser waveguide and then solved a stationary problem by applying the waveguide mode to the back-end of the laser waveguide. We used realistic complex index of refraction for different materials. Perfect matched layers were applied to all the boundaries of the simulation region to absorb all impinging waves [102]. The far-field emission pattern was calculated using near-field to far-field transformation algorithms based on the solution of electromagnetic fields on the boundary of the simulation area [102].

Fig. 4(a) shows a simulation of the intensity distribution for an unpatterned $\lambda_o = 9.9\ \mu\mathrm{m}$ QCL, demonstrating a large divergence of the original device. As a comparison, Fig. 4(b) shows a simulation of the intensity distribution for the device integrated with a plasmonic collimator of the second design with optimized geometry [Fig. 2(b)]. The simulation shows a central beam emerging from the aperture and many side beams emerging from the grating grooves. Fig. 4(c) is the calculated vertical far-field intensity distribution for the patterned device: the full-width at half-maximum (FWHM) divergence angle of the central beam is reduced to 3.7° for 15 grating grooves compared to about 60° of the original device. The optical background is relatively uniform as a function of angle and has an average intensity that is less than 10% of the peak intensity of the central lobe. Fig. 4(d) shows the distribution of electric field magnitude ($|E|$) around the slit and the first few grating grooves. The SPs are observed to be strongly localized to the patterned device facet, indicating strong coupling between the two; this is in striking contrast to the weak coupling between mid-IR SPs and a flat planar metallic surface. The latter case is demonstrated in Fig. 4(e), which shows the SPs loosely attached to the metal/air interface for a device with the slit aperture and no grating.

As discussed before, the reduction in far-field divergence is essentially an antenna array effect. Simulations show that the divergence angle scales inversely proportional to N at least up to $N = 60$ [Fig. 5(a)]. The peak intensity in the far-field scales approximately with the square of N up to $N = 25$ [Fig. 5(b)]. For $N > 25$, the effect of loss gives rise to a weaker variation of the peak intensity with N.

As mentioned at the end of Section II-A, fine-tuning of groove width and depth, w and h, is necessary to ensure that the length of the grating is about two to three times the SP propagation distance Γ_{SP}. Table I lists Γ_{SP} for different groove widths and depths for a $\lambda = 9.9\ \mu$m device. Γ_{SP} is calculated by fitting the distribution of SPs ($|E|$) on the patterned laser facet with an exponential function proportional to $\exp(x/\Gamma_{\mathrm{SP}})$, where x is the distance. It is observed from Table I that as h increases from

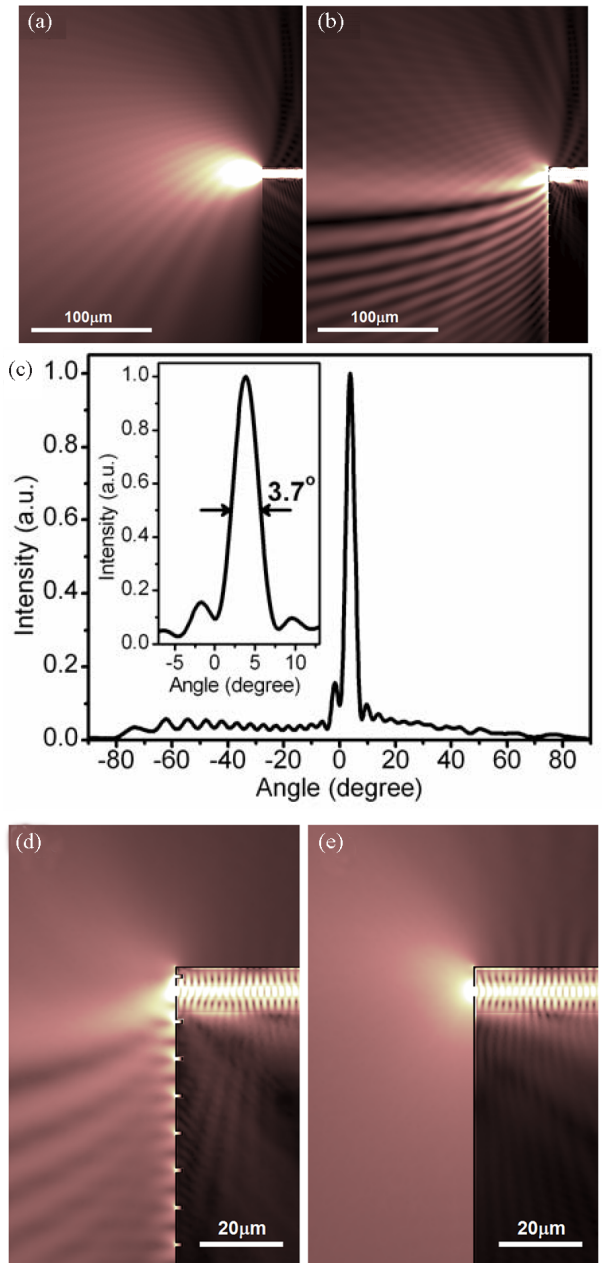

Fig. 4. (a) 2-D simulation showing the intensity distribution of an original unpatterned QCL emitting at $\lambda_o = 9.9\ \mu\mathrm{m}$. The simulation plane is perpendicular to the laser material layers and along the middle of the waveguide ridge. (b) 2-D simulation showing the intensity distribution of the QCL patterned with a plasmonic collimator containing 15 grating grooves. (c) Calculated far-field intensity distribution of the device shown in (b). Inset: zoom-in view of the central lobe. (d) Simulation of the electric field magnitude distribution around the slit and the first seven grating grooves. (e) Simulation of the electric field magnitude distribution for a $\lambda_o = 9.9\ \mu\mathrm{m}$ QCL with the slit aperture and no grating. The optimized values for $\lambda_o = 9.9\ \mu\mathrm{m}$ QCLs and a grating with 15 grooves are: $s = 2\ \mu$m, $\Lambda = 8.9\ \mu$m, $w = 0.8\ \mu$m, $h = 1.5\ \mu$m, $d_1 = 7.3\ \mu$m, and $d_{\mathrm{ref}} = 3.5\ \mu$m. The thicknesses of the alumina insulating layer and the gold layer are 200 and 400 nm, respectively. Their thicknesses on the walls of the grooves are 100 and 200 nm, respectively. The complex index of refraction of gold and alumina are $12.24 + 54.7i$ and $0.925 + 0.034i$, respectively, at $\lambda_o = 9.9\ \mu\mathrm{m}$, taken from [103] and [104]. The complex index of refraction of semiconductor layers constituting the laser waveguide are calculated based on the Drude model considering their doping levels (active region: $3.26 + 6.43 \times 10^{-4}i$; InGaAs cladding layers: $3.33 + 5.059 \times 10^{-4}i$; InP cladding layers: $3.02 + 9.52 \times 10^{-4}i$; InP substrate: $2.44 + 3.53 \times 10^{-2}i$). For the geometry and doping levels of the semiconductor layers for the $\lambda_o = 9.9\ \mu\mathrm{m}$ QCLs, see [83].

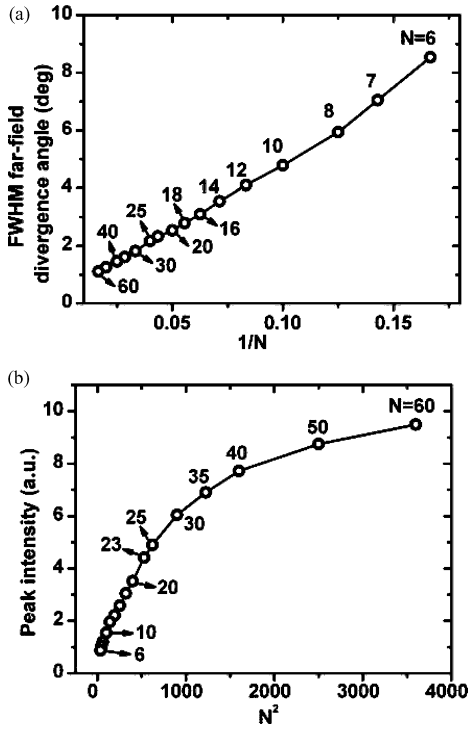

Fig. 5. (a) Simulation results showing the relation between far-field divergence angle and $1/N$, the inverse of the number of grating grooves. (b) Simulation results showing the relation between peak intensity of the far-field and N^2.

TABLE I
SP PROPAGATION DISTANCE Γ_{SP} FOR DIFFERENT GROOVE WIDTHS AND DEPTHS (GRATING PERIOD = 8.9 μm)

Γ_{sp} at λ=9.9 μm (μm)		w (μm)				
		0.5	0.6	0.8	1.0	1.5
h (μm)	1.1	2630	2050	1320	429	123
	1.2	1960	1113	436	207	74
	1.3	570	296	200	108	35
	1.5	220	146	45	21	9

1.1 to 1.5 μm, approaching the cavity resonance condition [87], [98], Γ_{SP} decreases dramatically due to significant enhancement of the scattering efficiency of the grooves. A similar effect is observed when w increases. Consequently, when designing a collimator with a relatively small number of grooves, say, $N = 15$ [Fig. 4(b) and (c)], we chose $w = 0.8$ μm and $h = 1.5$ μm, so that the length of the grating ($\approx$134 μm) is about three times Γ_{SP} (≈ 45 μm); while for a collimator with $N = 70$, we chose smaller groove width and depth, $w = 0.6$ μm and $h = 1.3$ μm, so that SPs propagate further and the length of the grating ($\approx$623 μm) is about twice Γ_{SP} (≈ 296 μm). The magnitude of SPs (the electric field $|E|$) 500 nm above the device facet for the latter case is shown in Fig. 6 as the red (light) curve. Also shown in the figure is $|E|$ for a structure with only the aperture (black or dark curve). Note that in a fairly large range near the aperture (distance $< \sim$350 μm), $|E|$ is larger in the former case than in the latter, demonstrating the ability of the grating to couple direct laser emission into SPs. The far-field divergence angle of this device is only about 1° and the optical background that is below 3% of the peak intensity (Fig. 6 inset).

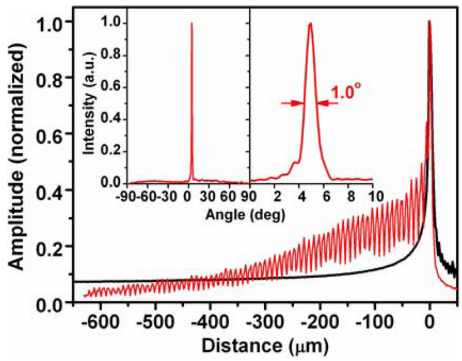

Fig. 6. Red (light) curve: calculated magnitude of SPs ($|E|$) 500 nm above a device facet with 70 grooves ($w = 0.6$ μm and $h = 1.3$ μm). Black (dark) curve: calculated magnitude of SPs 500 nm above a device facet without the grating. Distance = 0 corresponds to the location of the aperture; the grating is located at distance <0. Inset (−90° to +90° view and zoom-in view): calculated far-field intensity distribution for the device with 70 grooves.

C. Fabrication and Measurements

We fabricated the two types of devices depicted in Fig. 2. For the first design [Fig. 2(a)], the device facet is first coated with a layer of electrically insulating alumina (200 nm in thickness), followed by a layer of gold (1.7 μm in thickness) using electron-beam evaporation. Focused ion beam (FIB) milling is then used to define the slit-grating structure in the gold layer. For the second design [Fig. 2(b)], the grating grooves are first defined on the bare device facet using FIB, the insulating alumina and gold films are then deposited, and finally, the slit aperture is opened with FIB. A two-angle deposition procedure is used to coat both walls of the grooves. The thickness of alumina and gold on the laser facet is 200 and 400 nm, respectively, while their thicknesses on the walls of the grooves are about 100 and 200 nm, respectively.

To map the 2-D far-field emission patterns of the devices, we used a setup consisting of two motorized rotation stages. The devices tested were mounted on one of the rotation stages and could be rotated in the vertical plane. A mid-IR mercury–cadmium–telluride detector was mounted on the other stage and could be scanned in the horizontal plane. The distance between the devices and the detector was kept constant around 15 cm. Our measurements were performed with a resolution of about 0.25°. Power measurements were carried out with a calibrated power meter. The power meter had a metallic collection tube with a diameter of 6.5 mm and was placed within 2 mm of the laser facets, thus collecting emitted power in an angular range of approximately ±60° with respect to the normal of the laser facet. A Fourier-transform IR spectrometer was used for spectral measurements.

D. Experimental Results

Fig. 6(a) and (d) shows SEM images of two $\lambda_o = 9.9$ μm QCLs before and after patterning the 1-D plasmonic collimator of the second design. The 2-D far-field intensity distributions measured before and after patterning plasmonic structures are presented in Fig. 7(b), (c), (e), and (f), demonstrating a strong

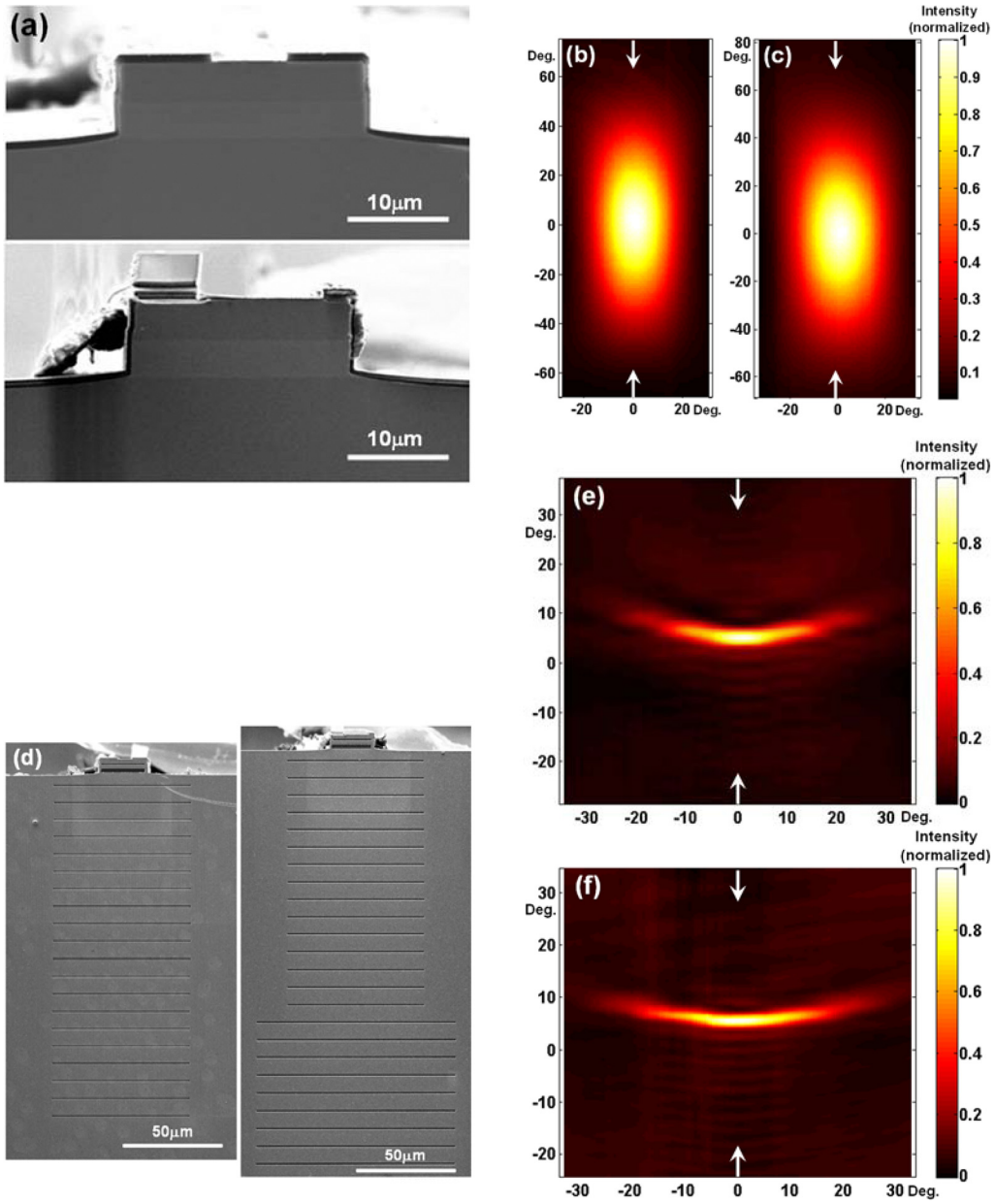

Fig. 7. (a) SEM images of the facets of two unpatterned QCLs emitting at $\lambda_o = 9.9\ \mu\mathrm{m}$. Device A (upper panel) has a ridge that is 25 μm wide and 2 mm long. Device B (lower panel) has a ridge that is 22 μm wide and 2 mm long. (b) and (c) Measured 2-D far-field intensity distributions of the unpatterned devices A and B, respectively. (d) SEM images of the facets of devices A and B patterned with 1-D plasmonic collimators of the second design [Fig. 2(b)]. Device A (left panel) has 20 grating grooves. Device B (right panel) has 24 grating grooves. (e) and (f) Measured 2-D far-field intensity distributions of devices A and B patterned with the plasmonic collimators, respectively. (Figures adapted from [83].)

reduction of the beam divergence in the vertical direction. The slight curvature of the far-field patterns in Fig. 7(e) and (f) is an edge effect due to the finite lateral size of the slit aperture.[1] The effect has been verified numerically by 3-D simulations of the entire structure and will be reported in a future publication [105].

[1]The finite size of the slit aperture in the lateral direction introduces lateral components in the SP wave vector (k_{SP}), reducing the vertical components $k_{\mathrm{SP}\perp}$ compared to the case of an infinitely wide slit, where $k_{\mathrm{SP}\perp}$ equals k_{SP}. This produces a wave vector mismatch ($k_{\mathrm{SP}\perp} < 2\pi/\Lambda$) leading to a small beam deflection toward the top of the device.

The line scans of the 2-D far-field emission patterns in the vertical direction are provided in Fig. 8(a)–(c), which show that the divergence angle is reduced from about 62° to about 2.9° for the device with 20 grating grooves, and from about 63° to about 2.4° for the device with 24 grating grooves. The line scans also show that the average intensity of the background of the two devices is below 10% of the peak value of the central lobe, which is an improvement compared to the devices of the first design [Fig. 9(b)]. This is possibly due to the improved quality of the grating grooves when they are sculpted directly into the

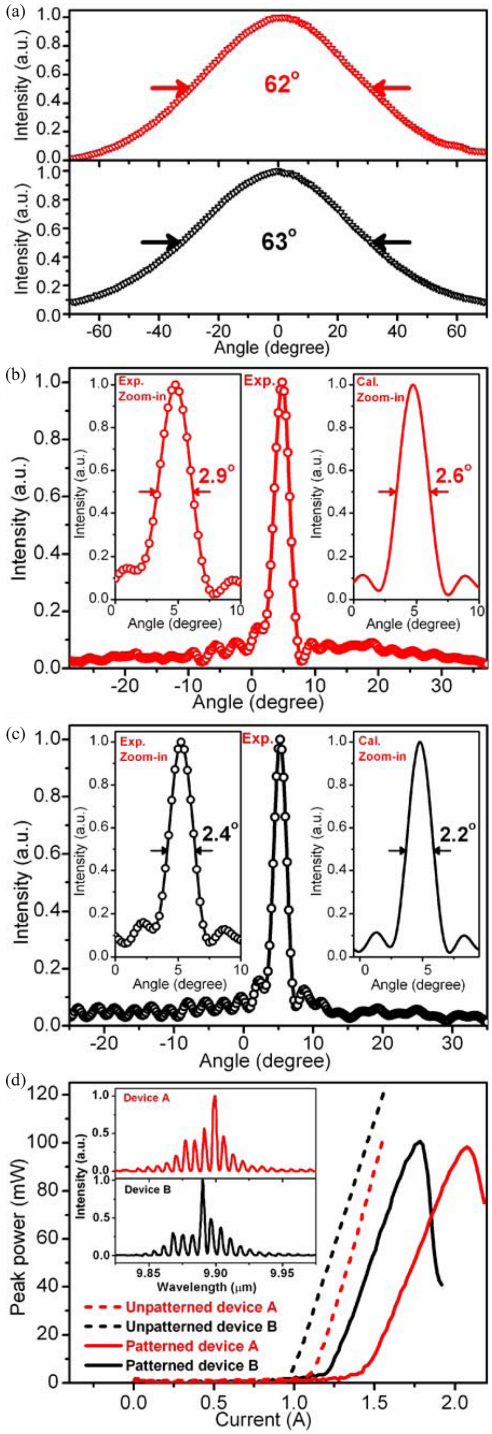

Fig. 8. (a) Upper and lower panels are vertical line scans of Fig. 7(b) and (c) along the arrows, respectively. (b) and (c) Vertical line scans of Fig. 7(e) and (f) along the arrows, respectively. Left and right insets are the zoom-in views of the experimental and the calculated central lobe of the line scans, respectively. (d) Dashed and solid curves are *LI* curves of the unpatterned and patterned devices, respectively. The red (light) and black (dark) curves correspond, respectively, to devices A and B in Fig. 7(d). Inset: laser spectra of devices A (upper panel, $I = 1.8$A) and B (lower panel, $I = 1.5$ A). In all the measurements, the lasers are operated at room temperature in pulsed mode with 80-kHz repetition rate and 125-ns pulse duration. Note that in the measurement of *LI* curves, the power meter collects laser emission in an angular range of approximately $\pm 60^{\circ}$ with respect to the normal of the laser facet. This will include the main lobe of the far-field as well as part of the optical background. For the devices shown in Fig. 7(d), the main lobe of the far-field [Fig. 7(e) and (f)] contains approximately 70% of the collected power. (Figures adapted from [83].)

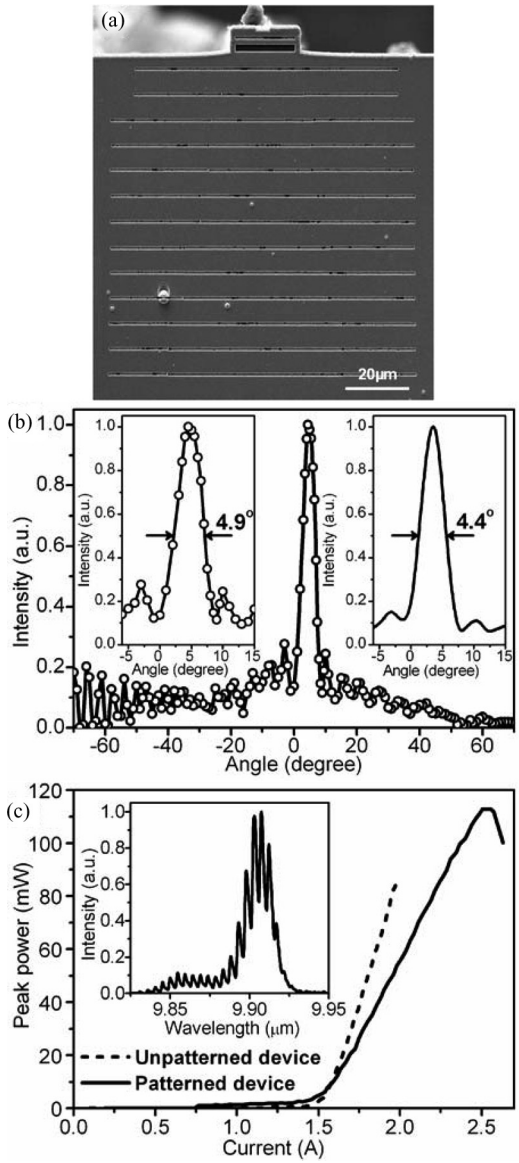

Fig. 9. (a) SEM image of a 22-μm-wide, 3-mm-long, $\lambda_o = 9.9\ \mu$m QCL with a 1-D plasmonic collimator of the first design [Fig. 2(a)]. There are 13 grating grooves. Roughness can be observed on the bottom of the grating grooves: the dark spots are holes on the gold film exposing the alumina layer underneath. (b) Measured vertical far-field intensity distribution of the device; left and right insets are the zoom-in views of the experimental and the calculated central lobe, respectively. (c) *LI* curves taken before (dashed line) and after (solid line) defining the collimator. Inset: laser spectrum of the device with the plasmonic collimator taken at $I = 2.2$ A. In all the measurements, the laser is operated at room temperature in pulsed mode with 80-kHz repetition rate and 125-ns pulse duration. (Figures adapted from [83].)

semiconductor; it is observed consistently in experiments that devices of the first design give larger background light compared to those of the second design. We note that there is no noticeable damage to the metallic collimators after high-peak-power operation. The beam quality factor M^2 (i.e., the factor by which the divergence angle of a laser beam is larger than that of a Gaussian beam, assuming the two have the same beam waist) of the device with 24 grating grooves is determined to be about 2.5 based on measurements of the variation of the beam

waist along the propagation direction. We find from Fig. 8(b) and (c) that the directivity D is about 17.7 and 18.3 dB for the two devices with 20 and 24 grooves, respectively, while D is only about 7.2 dB for the original unpatterned lasers.

The QCLs used in our experiment operate on the fundamental TM_{00} transverse mode. The lateral beam divergence after definition of the collimators is similar to that of the original lasers; this is because the grating is a 1-D structure, so that beam divergence is greatly reduced only in the direction perpendicular to the grooves.

Fig. 8(d) shows the light output versus current (*LI*) characteristics before and after defining the plasmonic structure, demonstrating a maximum output power of about 100 mW. The slope efficiency of the *LI* characteristics of the patterned devices is proportional to $\eta\alpha_{\rm m}/(\alpha_{\rm m}+\alpha_{\rm w})$, where η is the efficiency of the plasmonic grating to couple SPs into propagating waves, $\alpha_{\rm m}$ is the mirror loss, and $\alpha_{\rm w}$ is the waveguide loss. We found that larger slope efficiencies correlate with gratings with a larger number of grooves: devices with 24 grooves had a slope efficiency of about 180 mW/A, which is approximately 90% of that of the original laser; devices processed the same way but with only 15 grooves had a slope efficiency of only about 120 mW/A, indicating incomplete coupling of SPs into the far-field. The increase of the threshold current [Fig. 8(d)] for the devices of the second design is probably due to leakage currents between the device top contact and the gold coating (which is electrically connected to the substrate) through the thin alumina layer. An improved fabrication process using a thicker alumina insulating layer would prevent this. The change in threshold due to the change of the effective reflectivity of the facet patterned with a slit aperture is small; we observed consistently that for several devices of the first design, the current threshold showed minor variations [for example, see Fig. 9(c)], meaning that the addition of the collimator does not significantly change the effective reflectivity of the facet or the mirror loss $\alpha_{\rm m}$. The slope efficiency of the device shown in Fig. 9(a) is less than that of the original device [Fig. 9(c)], probably due to the limited number of the grating grooves and scattering of SPs by the roughness on the plasmonic collimator [Fig. 9(a)].

We demonstrated experimentally that the divergence angle is roughly inversely proportional to N, the number of grating grooves. Fig. 10 shows vertical far-field intensity profiles of devices patterned with different number of grating grooves. Both simulations [Fig. 10(a) and (c)] and experimental results [Fig. 10(b) and (d)] are presented, and there is a good agreement between the two sets of data. Devices with larger N have smaller average background and narrower collimation angles.

III. 2-D Collimation

A. Design

The grating discussed in Section II extends only in the laser polarization direction. The lateral dimension of the slit aperture is several times larger than the free-space wavelength λ_o, so that the SPs propagate mainly in the direction perpendicular to the aperture slit, giving rise to overlapping between the SPs and the

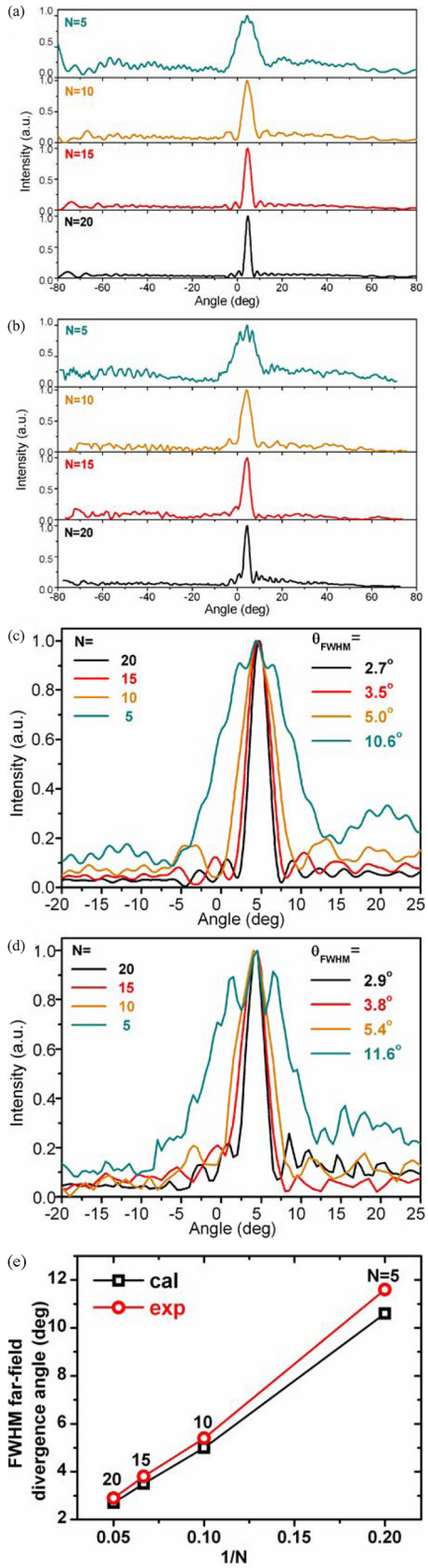

Fig. 10. (a) and (b) Simulated and measured vertical far-field intensity distribution of devices of the second design [Fig. 2(b)] with different number of grating grooves N. (c) and (d) Zoom-in views of (a) and (b), respectively. (e) Simulation and experimental results showing that the far-field divergence angle is roughly proportional to $1/N$.

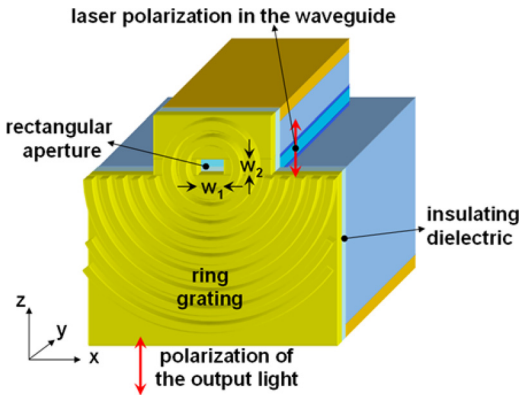

Fig. 11. Sketch of the small-divergence device, consisting of a QCL and a metallic aperture–grating structure defined on its facet.

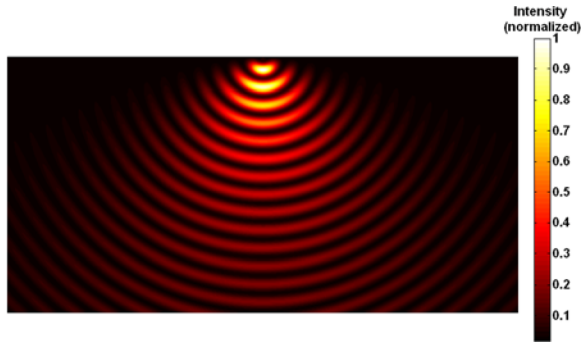

Fig. 12. Calculated instantaneous SP distribution ($|E|^2$) around an infinitesimal aperture defined on a uniform gold film. The SPs are monitored on a plane 100 nm above the metal surface. The wavelength is assumed to be 8 μm. Area in display: $60 \times 120\ \mu\mathrm{m}^2$.

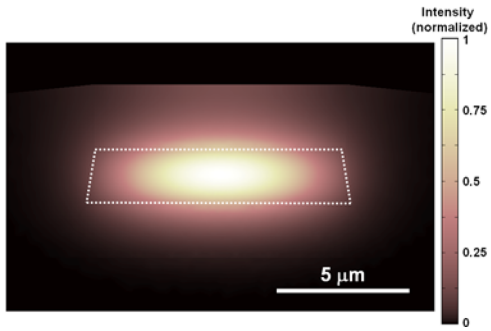

Fig. 13. Simulation showing the intensity of the electric field ($|E|^2$) of the fundamental TM_{00} mode in the laser waveguide. The dotted lines indicate the boundaries of the laser active region.

1-D grating. As a result, beam collimation is only realized in one direction.

We further develop this idea to design an aperture that can launch SPs in two dimensions and design a 2-D plasmonic pattern that can coherently scatter the 2-D SPs into the far-field. This could lead to constructive interference not only in the vertical direction but also in the lateral direction, thus achieving complete collimation in the plane perpendicular to the laser beam. Several plasmonic structures can satisfy the requirements; we choose a relatively simple design consisting of a rectangular aperture and a concentric half-ring grating (Fig. 11).

Now, we discuss the physical considerations used to choose the shape and the dimension of the aperture. The choice of other design parameters follows arguments similar to those discussed in Section II, including the grating period Λ, the distance between the aperture and the first groove d_1 (i.e., the radius of the first ring r_1), and the depth h and width w of the grooves.

1) Aperture Shape and Dimension: For 2-D collimation, it is crucial to efficiently propagate SPs in both the vertical and lateral directions on the laser facet (z- and x-axes in Fig. 11). SPs propagate preferentially in the vertical direction because QCLs are TM-polarized. To achieve broad diffraction of SPs in the lateral direction, the lateral dimension of the aperture has to be at subwavelength level. Ideally, if the dimensions of the aperture are much smaller than λ_o, the aperture functions effectively as a point source of SPs: the SP intensity follows a $(\cos\theta)^2$ profile and the FWHM divergence angle of SPs is 90° [106]–[108] (Fig. 12). Here, θ is the angle from the laser polarization direction. However, a small aperture strongly scatters laser beam back into laser cavity, thus severely limiting the device power throughput. A larger aperture increases the mirror loss and accordingly increases the slope efficiency of the lasers, enabling the devices to reach higher maximum optical power; however, as the aperture size is increased, the point-source approximation is no longer valid and the divergence of the SPs, governed by diffraction, progressively decreases. This results in less efficient collimation in the lateral direction. A tradeoff is thus to be sought between power throughput and collimation.

QCLs used to demonstrate 2-D collimation operate in the fundamental TM_{00} mode: the laser mode profile is elliptical, determined by the laser waveguide (Fig. 13). We choose a rectangular aperture because it permits good overlap with the mode profile. By increasing the lateral size of the rectangular aperture w_1 in steps, one can study the relation between power throughput and lateral collimation. The vertical aperture size w_2 is maintained to be approximately equal to the thickness of the laser active region: a smaller w_2 would limit the power throughput while larger w_2 would result in reduced efficiency of coupling into SPs and increased optical background in the far-field.

We note that the SP wavefront is circular for a rectangular aperture (w_1 varying between 2 and 10 μm, and w_2 equal to 2 μm), as confirmed by our simulations. This allows the circular grating grooves to match the SP wavefront.

B. Simulations

We performed systematic 3-D simulations to study the evolution of the power outflow and the SP divergence as a function of the lateral aperture size w_1. Fig. 14(a) is a simulation result showing the intensity ($|E|^2$) of the SPs for a device with a $w_1 \times w_2 = 4 \times 2\ \mu\mathrm{m}^2$ aperture and 20 circular grating grooves (rings). The SPs spread widely on the laser facet. In Fig. 14(b), the simulation results for devices with different w_1 and 20 rings are summarized. The red (light) curve in Fig. 14(b) shows that

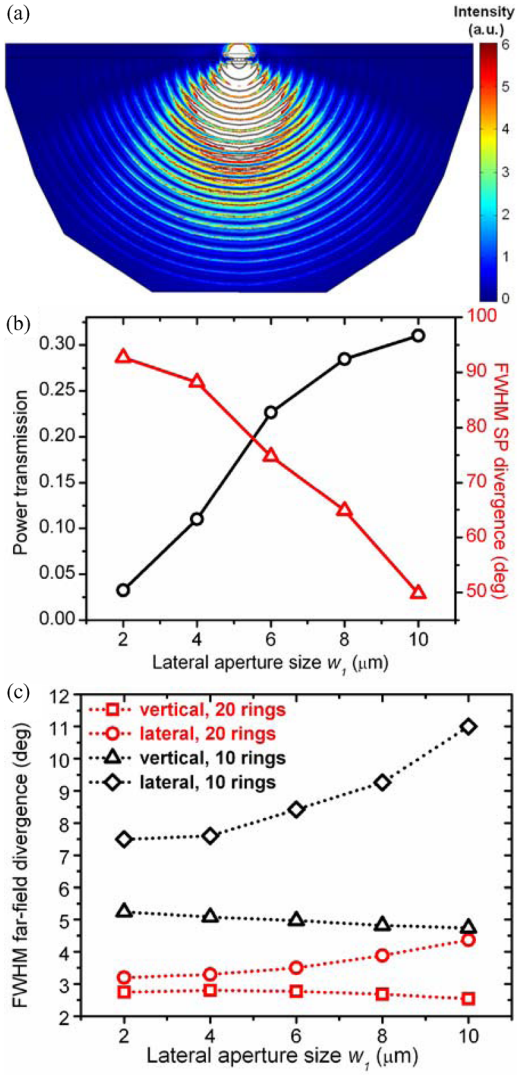

Fig. 14. (a) Simulation showing the intensity distribution of the SPs. The SPs are highly localized on the device facet: their half-intensity decay point is approximately 3 μm away from the facet. Shown is $|E|^2$ at 100 nm above the laser facet. (b) Simulated FWHM SP dispersion angle and power throughput as a function of the lateral aperture size w_1 for a device with 20 circular grating grooves (rings). Power transmission is defined as all the transmitted power (including the far-field component and the near-field one that is not scattered into the far-field by the grating) divided by the power launched into the laser waveguide. As such, the power throughput is directly linked to the mirror loss of the patterned device facet. (c) Simulated far-field divergence angles in the vertical and lateral directions for the devices with 10 and 20 rings. In all the simulations, the vertical aperture size w_2 is kept constant at 2 μm. The complex index of refraction of gold and alumina are $8.62 + 46.67i$ and $1.36 + 0.0095i$, respectively, at $\lambda_o = 8.06$ μm, taken from [103] and [104]. The complex index of refraction of semiconductor layers constituting the laser waveguide are calculated based on the Drude model considering their doping levels (active region: $3.28 + 1.29 \times 10^{-4}i$; InGaAs cladding layers: $3.33 + 9.11 \times 10^{-4}i$; InP cladding layers: $3.05 + 5.10 \times 10^{-4}i$; InP substrate: $2.68 + 1.74 \times 10^{-2}i$). For the geometry and doping levels of the semiconductor layers for the $\lambda_o = 8.06$ μm QCLs, see [109]. (Figures adapted from [85].)

a small aperture (2×2 μm^2) gives an FWHM SP intensity divergence angle very close to 90°, which is consistent with the prediction of the $(\cos\theta)^2$ rule. There is still significant lateral propagation of SPs when w_1 is nearly equal to $\lambda_o = 8.06$ μm, while the power throughput is greatly improved [a factor of 10

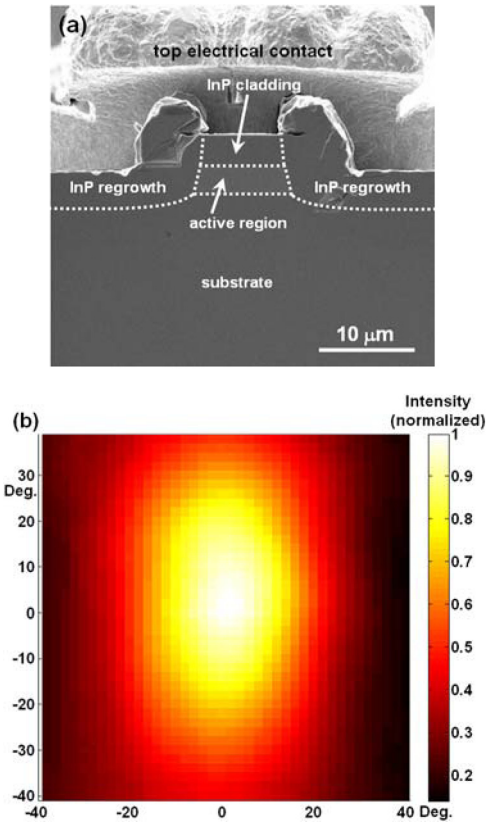

Fig. 15. (a) SEM image showing the facet of an unpatterned $\lambda_o = 8.06$ μm BHT QCL. (b) 2-D far-field intensity profile of the device. (Figures adapted from [85].)

compared to an aperture with $w_1 = 2$ μm; see the black (dark) curve in Fig. 14(b)]. Fig. 14(c) shows the calculated far-field divergence angles in the vertical and lateral directions at different lateral aperture size w_1 for the devices patterned with 10 and 20 rings. Note that as w_1 increases from 2 to 10 μm, the lateral divergence angle $\theta_{||}$ increases by approximately 50% due to the narrowing of the SP divergence angle on the laser facet, as presented in Fig. 14(b). At the same time, the vertical divergence angle $\theta_\perp$ decreases slightly; this is probably due to improved propagation of SPs in the vertical direction as the aperture widens up.

C. Devices and Fabrication

We fabricated 2-D plasmonic collimators on both buried heterostructure (BHT) QCLs [Fig. 15(a)] and ridge QCLs. BHT device has regrown regions on the lateral sides of the laser active core [Fig. 15(a)]; it is more efficient in heat removal compared with ridge devices. The regrown regions also provide lateral electrical and optical confinement. The ridge devices used in our experiments lase at $\lambda_o = 9.95$ μm and are grown by molecular beam epitaxy; the BHT devices used lase at $\lambda_o = 8.06$ μm and are grown by metal–organic vapor-phase epitaxy [109]. The ridge devices have 2.1-μm-thick active regions and various lateral active-region widths. The active region of all the BHT devices used has a cross section of 2.1 μm $\times$ 9.7 μm in the vertical and lateral directions.

The fabrication procedure is similar to the second design of the 1-D collimators reported in Section II.

D. Experimental Results

A detailed study was performed for $\lambda_o = 8.06\ \mu\mathrm{m}$ BHT QCLs patterned with 2-D plasmonic collimators. The original devices with unpatterned facets have divergence angles of $\theta_{||} = 42^\circ$ and $\theta_\perp = 74^\circ$ [Fig. 15(b)]. Fig. 16(a) and (c) show two representative devices patterned with 10 and 20 rings and with small aperture sizes $w_1 \times w_2 = 2.8 \times 1.9\ \mu\mathrm{m}^2$ and $2.1 \times 1.9\ \mu\mathrm{m}^2$, respectively. The far-field intensity profiles are shown in Fig. 16(b) and (d) for the two devices, respectively. Compared to the unpatterned devices, the ones patterned with the 2-D collimators exhibit greatly reduced divergence angle: $\theta_{||}$ and $\theta_\perp$ are 8.6° and 5.1° for the device with 10 rings and 3.7° and 2.7° for the device with 20 rings. By comparing Fig. 16(b) and (d), one sees that the device with 10 rings has a larger optical background outside of the central beam than the device with 20 rings. While the directivity D is only about 8.3 dB for the unpatterned lasers, it is about 17.3 and 26.9 dB for the devices with 10 and 20 rings, respectively. The beam quality factor (M^2 factor) of the device with 20 rings is about 2.0 in both vertical and lateral directions based on measurements of the variation of the beam waist along the propagation direction.

The BHT devices used for 2-D collimation operate on multiple longitudinal modes: the central wavelength is at $\lambda_o = 8.06\ \mu\mathrm{m}$ and the spectrum width $\Delta\lambda$ usually broadens at a large driving current I_{dr} (Fig. 17). For example, for the device patterned with 10 ring grooves and a $2.8 \times 1.9\ \mu\mathrm{m}^2$ aperture, $\Delta\lambda$ is approximately 0.1 μm at $I_{\mathrm{dr}} = 500\ \mathrm{mA}$; it quickly increases to about 0.2 μm at $I_{\mathrm{dr}} = 600\ \mathrm{mA}$ and stays around 0.2 μm at larger I_{dr} up to 1.0 A [Fig. 17(a)]. The spectral broadening raises reliability issues for plasmonic collimation. As discussed in Section II, the lasing wavelength is the central factor determining all the other design parameters: it determines the surface wave wavelength λ_{sw}, and therefore, the optical grating geometries ($d_1, \ldots, d_n$, and d_{ref}); the groove width w and depth d are also optimized only for this particular wavelength. Fortunately, we found that the far-field characteristics were rather insensitive to these spectral changes. For instance, we measured that for the device with 10 rings, $\theta_\perp$ equals to 5.0°, 5.1°, and 5.1°, and $\theta_{||}$ equals to 8.5°, 8.6°, and 8.6° at $I_{\mathrm{dr}} = 500$, 600, and 800 mA, respectively; for the device with 20 rings, $\theta_\perp$ equals to 2.6° and 2.7°, while $\theta_{||}$ remains at 3.7° at $I_{\mathrm{dr}} = 500$ and 600 mA, respectively. The directivities D were found to be nearly constant as a function of I_{dr}. To understand this phenomenon, we conducted simulations and analytical calculations to investigate the impact of spectrum broadening on beam divergence. Simulations show that a shift of lasing wavelength by 0.1 μm gives rise to a 1° shift to the far-field direction angle. However, the center wavelength of new spectra experiences negligible shift with increasing driving current (Fig. 17); analytical calculations estimate that there is only a minor increase of about 0.3° of the FWHM far-field divergence angles if $\Delta\lambda$ equals 0.2 μm.

We increased the aperture lateral size w_1 of the aforementioned devices stepwise using FIB milling to investigate its

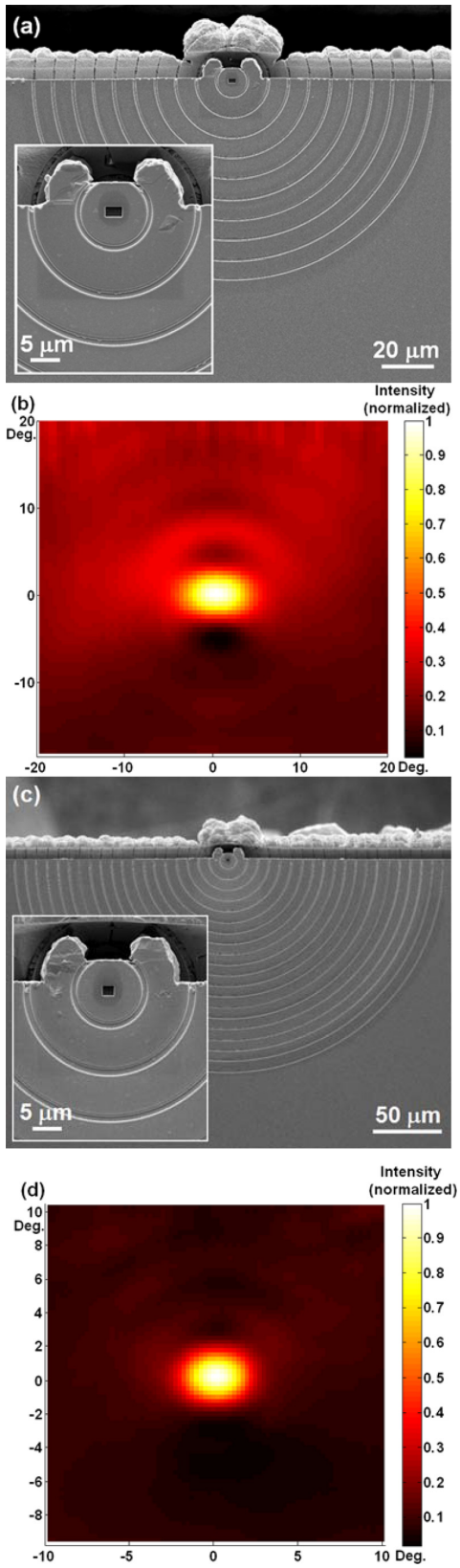

Fig. 16. (a) and (c) SEM images of the two devices patterned with 10 and 20 rings, respectively. Insets are zoom-in views. The two devices have aperture sizes of $w_1 \times w_2 = 2.8 \times 1.9$ and $2.1 \times 1.9\ \mu\mathrm{m}^2$, respectively. (b) and (d) Measured 2-D far-field intensity profiles for the two devices, respectively. The far-field measurements were performed while the lasers were operated in pulsed mode with an 80-kHz repetition rate and 1% duty cycle. (Figures adapted from [85].)

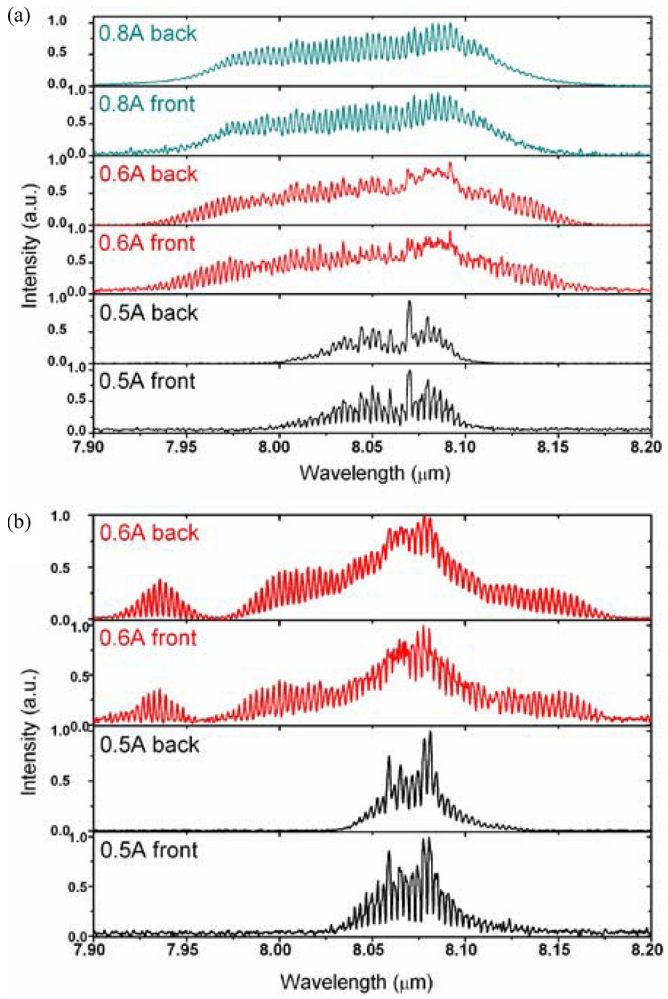

Fig. 17. Spectra of the device patterned with (a) 10 rings and (b) 20 rings. There is significant spectral broadening with increasing driving current. Spectra taken from both the front facet (patterned with the collimator) and the back facet (uncoated) are quite similar.

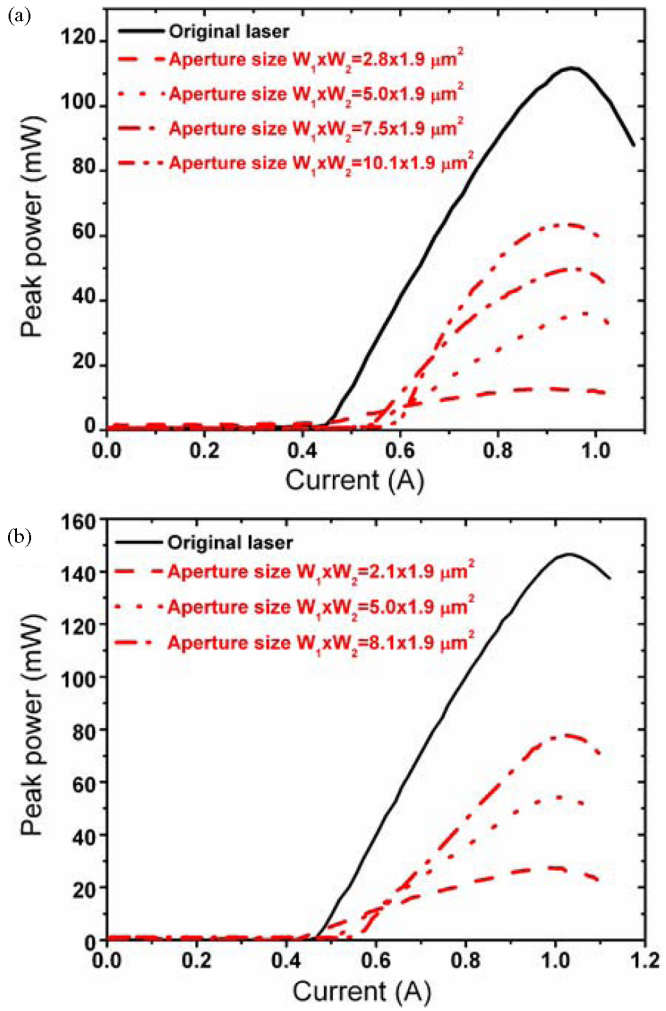

Fig. 18. *LI* characteristics for the two BHT devices. (a) and (b) For devices patterned with 10 and 20 rings, respectively. Solid lines are *LI* curves for the original unpatterned devices and other curves are taken after the devices have been patterned with collimators with various aperture sizes. In all the measurements, the lasers are operated at room temperature in pulsed mode with an 80-kHz repetition rate and 1% duty cycle. For the device with 20 rings, the main lobe of the far-field contains approximately 70% of the collected power, while for the device with 10 rings, which has larger background, the main lobe contains about 40% of the collected power. (Figures adapted from [85].)

impact on $\theta_{\perp}$, $\theta_{||}$, and the power output. The vertical aperture size w_2 was kept constant at 1.9 μm. The *LI* curves of the devices for different aperture sizes are shown in Fig. 18. As predicted by simulations [Fig. 14(b)], devices with a larger aperture have larger slope efficiency, and therefore, a higher maximum power. The *LI* curves also illustrate the dependence of the lasing threshold with w_1. A small aperture corresponds to the laser active core being mostly covered by gold. The effective reflectivity of the facet is therefore larger than that of the original devices, and correspondingly, its mirror loss is smaller, leading to a reduced lasing threshold. As w_1 increases, the device experiences a gradual increase of the lasing threshold, due to increased scattering loss at the aperture. The devices exhibit a larger threshold compared with the original devices when $w_1 = 5$ μm, about half of the active region width.

Fig. 19 summarizes the measured far-field beam divergence angles for different aperture sizes; as a comparison, the calculated values are also shown. It is observed that as w_1 increases, the lateral divergence angle $\theta_{||}$ increases due to the narrowing of the SP divergence on the laser facet, as shown in Fig. 14(b); on the other hand, $\theta_{\perp}$ essentially remains constant because the vertical propagation of SPs (i.e., along the laser polarization direction) is insensitive to these changes in aperture geometry. For the widest apertures investigated (10.1 μm for the device with 10 rings and 8.1 μm for the one with 20 rings), the maximum output power $P_{\max}$ was more than 50% of that of the original unpatterned laser, while the divergence angles are still significantly smaller than those of the original unpatterned devices. For instance, 53% of the original power was measured for the device with 20 rings [Fig. 18(b)], which has a divergence of only $\theta_{\perp} = 2.4^{\circ}$ and $\theta_{||} = 4.6^{\circ}$ (Fig. 19).

Fig. 19 shows that while there is a good agreement between the calculated and the measured vertical far-field divergence angles, the measured lateral divergence angles tend to be larger than the calculated values by about 20%. One possible reason for this discrepancy is that in the simulations, we did not take

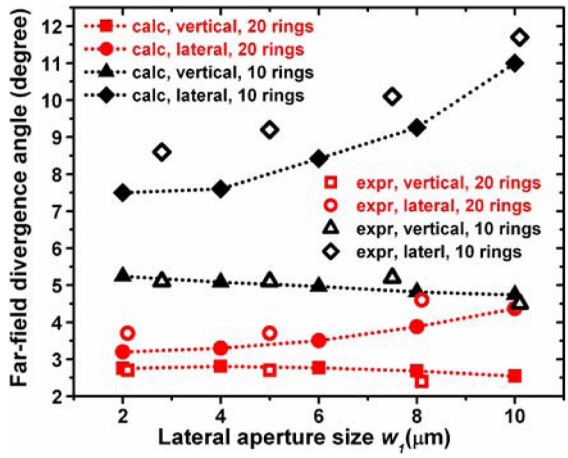

Fig. 19. Divergence angles in the vertical and lateral directions as a function of the lateral aperture size w_1. Calculation results are represented with filled symbols and experimental results are represented with hollow symbols. (Figure adapted from [85].)

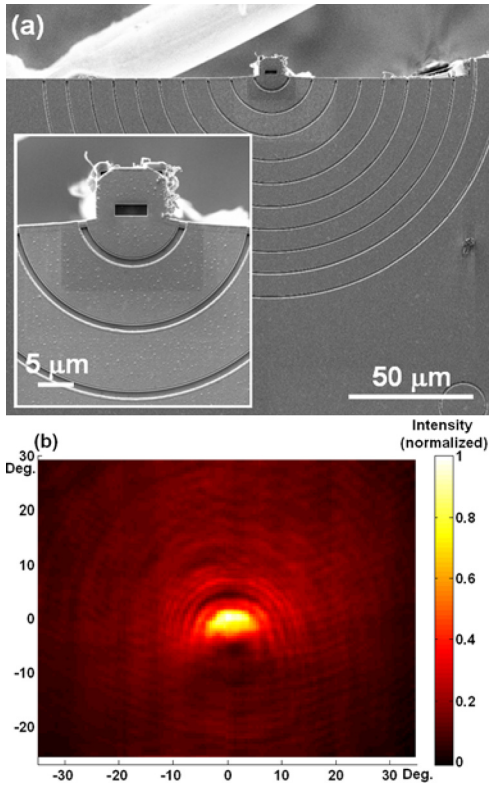

Fig. 20. (a) SEM image showing the device facet. Inset is a zoom-in view. (b) Measured far-field intensity profile for the device. The far-field measurements were performed while the lasers were operated in pulsed mode with an 80-kHz repetition rate and 1% duty cycle. (Figures adapted from [85].)

into consideration the detailed geometry of the InP regrown regions of the BHT lasers [Fig. 15(a)] and simply modeled the laser waveguide as rectangular. The two humps at the edges of the laser ridge, which are formed during regrowth of the ridges for BHT processing, are adjacent to the first ring groove [for instance, see Fig. 16(a)] and may scatter the SPs in an unpredictable manner, affecting their lateral spreading and eventually the lateral far-field divergence.

The processing of ridge waveguide semiconductor lasers is much easier compared with the BHT devices, which require the regrowth of semi-insulating side cladding layers. It is therefore instructive to show that the 2-D plasmonic collimator design also works for devices with ridge waveguides. Ridge QCLs have less facet area for patterning compared to the BHT devices; however, considering that SPs are mainly distributed along the vertical direction and that there is little SP propagation in the lateral direction, as demonstrated in Fig. 14(a), we expect that plasmonic-collimated ridge QCLs and BHT QCLs should function very similarly. Experimentally, we fabricated 2-D collimators on $\lambda_o = 9.95\ \mu\mathrm{m}$ ridge QCLs. The optimized design for this wavelength could be easily obtained by a scaling of the optimized structure for the $\lambda_o = 8.06\ \mu\mathrm{m}$ BHT devices. An SEM image of one representative ridge device with a ring collimator and its far-field emission profile are presented in Fig. 20. The performance of this device is comparable to the BHT devices with the same number of ring grooves: its divergence angles are $\theta_\perp = 5.0^\circ$ and $\theta_{||} = 8.1^\circ$, and its directivity D is about 16.2 dB.

IV. Future Directions

We plan to investigate optimized aperture shapes that could enhance the power throughput and couple laser light into SPs more efficiently. C-shaped [110]–[115] and H-shaped [116], [117] apertures allow high power transmission under resonance conditions and have a small footprint, which could give broad 2-D distribution of SPs on the laser facet (and therefore good collimation in the far-field). These specific apertures fall under the concept of slot antennas [118], which may be good candidates to function as highly confined, high-throughput structures. We also plan to make plasmonic collimators for visible or near-IR edge-emitting laser diodes and VCSELs. Our current design is most suitable for lasers with a small emission area such as edge-emitting devices; VCSELs have much larger emission facet, which demand a different design that does not strongly limit their power throughput. To make plasmonic collimation really useful, better fabrication techniques need to be explored. We have currently employed FIB milling for proof of concept, which is a high-cost and low-throughput process. We plan to use soft lithographic techniques, such as imprint lithography [119] and microcontact printing [120], to pattern our plasmonic structures. These methods allow parallel processes with high throughput and good cost-effectiveness.

In a broader scope, we envision designing and building plasmonic nanostructures or metamaterials on the facet of many types of semiconductor lasers and also on fiber lasers to achieve complex wavefront engineering, such as beam steering, Bessel beams, etc., as mentioned in Section I. On a more basic level, one can also use the device facet as an optical bench to study a variety of interesting properties of SPs. Our scheme of using the device facet as a platform to study SPs is optimal due to the high efficiency of coupling laser emission directly into SPs, which is unachievable in conventional experimental schemes.

V. Conclusion

Plasmonic collimation has many advantages over conventional collimation techniques. First, plasmonic collimators are integrated with lasers; thus, they require no alignment. Second, by proper scaling of the plasmonic collimator design according to wavelength and polarization, it can fit onto any type of semiconductor laser with a wide range of emitting wavelengths from visible to THz. Conventionally, to efficiently collect optical power emitted from semiconductor lasers, lenses with a large numerical aperture (NA) close to unity are needed. Plasmonic collimation coupled with a low-NA lens could become a cost-effective alternative solution. Lastly, the 2-D plasmonic collimator is essentially able to control the beam divergence in two orthogonal directions if different number of scattering elements in the vertical and lateral directions are used. This is helpful for some applications such as light detection and ranging, where a collimated beam with circular cross section is required to reduce aberration along the optical path.

In conclusion, we have performed systematic simulations and experiments to demonstrate that the integration of a suitably designed 1-D or 2-D plasmonic structure on the facet of QCLs reduces the beam divergence by more than one orders of magnitude, in one direction or two orthogonal directions. The optimized devices preserve a high output power, comparable to that of the unpatterned lasers. We have shown that the 2-D plasmonic collimator design is applicable to both BHT and ridge devices.

Acknowledgment

The authors gratefully acknowledge the Center for Nanoscale Systems (CNS) at Harvard University. Harvard CNS is a member of the National Nanotechnology Infrastructure Network. The authors would like to thank H. Mosallaei for helpful discussions and suggestions.

References

[1] A. E. Siegman, *Lasers*. Sausalito, CA: Univ. Science Books, 1986, ch. 18, pp. 712–743.

[2] A. Yariv and P. Yeh, *Photonics: Optical Electronics in Modern Communications*, 6th ed. Oxford, U.K.: Oxford Univ. Press, 2007, ch. 16, pp. 719–720; ch. 1, pp. 47–51.

[3] H. C. Liu and F. Capasso, *Intersubband Transitions in Quantum Wells: Physics and Device Applications I*. San Diego, CA: Academic, 2000, ch. 1, p. 8.

[4] M. Troccoli, C. Gmachl, F. Capasso, D. L. Sivco, and A. Y. Cho, "Mid-infrared ($\lambda \approx 7.4\ \mu$m) quantum cascade laser amplifier for high-power single-mode emission and improved beam quality," *Appl. Phys. Lett.*, vol. 80, pp. 4103–4105, Jun. 2002.

[5] L. Nähle, J. Semmel, W. Kaiser, S. Höfling, and A. Forchel, "Tapered quantum cascade lasers," *Appl. Phys. Lett.*, vol. 91, pp. 181122-1–181122-3, Nov. 2007 (Erratum: *Appl. Phys. Lett.*, vol. 92, p. 019904-1, Jan. 2008).

[6] H. Soda, K. Iga, C. Kitahara, and Y. Suematsu, "GaInAsP/InP surface emitting injection lasers," *Jpn. J. Appl. Phys.*, vol. 18, pp. 2329–2330, 1979.

[7] H. Kogelnik and C. V. Shank, "Coupled-wave theory of distributed feedback lasers," *J. Appl. Phys.*, vol. 43, pp. 2327–2335, May 1972.

[8] R. J. Noll and S. H. Macomber, "Analysis of grating surface emitting lasers," *IEEE J. Quantum Electron.*, vol. 26, no. 3, pp. 456–466, Mar. 1990.

[9] Y. Kan, Y. Honda, I. Suemune, and M. Yamanishi, "Electronic beam deflection in a semiconductor laser diode using grating output coupler," *Electron. Lett.*, vol. 22, pp. 1310–1311, Nov. 1986.

[10] K. Kojima, S. Noda, K. Mitsunaga, K. Kyuma, and K. Hamanaka, "Continuous wave operation of a surface-emitting AlGaAs/GaAs multiquantum well distributed Bragg reflector laser," *Appl. Phys. Lett.*, vol. 50, pp. 1705–1707, Jun. 1987.

[11] G. A. Evans, N. W. Carlson, J. M. Hammer, M. Lurie, J. K. Butler, S. L. Palfrey, R. Amantea, L. A. Carr, F. Z. Hawrylo, E. A. James, C. J. Kaiser, J. B. Kirk, and W. F. Reichert, "Coherent, monolithic two-dimensional (10×10) laser arrays using grating surface emission," *Appl. Phys. Lett.*, vol. 53, pp. 2123–2125, Nov. 1988.

[12] N. W. Carlson, G. A. Evans, R. Amantea, S. L. Palfrey, J. M. Hammer, M. Lurie, L. A. Carr, F. Z. Hawrylo, E. A. James, C. J. Kaiser, J. B. Kirk, and W. F. Reichert, "Electronic beam steering in monolithic grating-surface-emitting diode laser arrays," *Appl. Phys. Lett.*, vol. 53, pp. 2275–2277, Dec. 1988.

[13] G. A. Evans, N. W. Carlson, J. M. Hammer, M. Lurie, J. K. Butler, S. L. Palfrey, R. Amantea, L. A. Carr, F. Z. Hawrylo, E. A. James, C. J. Kaiser, J. B. Kirk, and W. F. Reichert, "Two-dimensional coherent laser arrays using grating surface emission," *IEEE J. Quantum Electron.*, vol. 25, no. 6, pp. 1525–1538, Jun. 1989.

[14] D. F. Welch, R. Parke, A. Hardy, R. Waarts, W. Streifer, and D. R. Scifres, "High-power, 4 W pulsed, grating-coupled surface-emitting laser," *Electron. Lett.*, vol. 25, no. 16, pp. 1038–1039, Aug. 1989.

[15] J. D. Mott and D. H. Macomber, "Two-dimensional surface emitting distributed feedback laser arrays," *IEEE Photon. Technol. Lett.*, vol. 1, no. 8, pp. 202–204, Aug. 1989.

[16] G. A. Evans, D. P. Bour, N. W. Carlson, J. M. Hammer, M. Lurie, J. K. Butler, S. L. Palfrey, R. Amantea, L. A. Carr, F. Z. Hawrylo, E. A. James, J. B. Kirk, S. K. Liew, and W. F. Reichert, "Coherent, monolithic two-dimensional strained InGaAs/AlGaAs quantum well laser arrays using grating surface emission," *Appl. Phys. Lett.*, vol. 55, pp. 2721–2723, Dec. 1989.

[17] G. A. Evans, D. P. Bour, N. W. Carlson, R. Amantea, J. M. Hammer, H. Lee, M. Lurie, R. C. Lai, P. F. Pelka, R. E. Farkas, J. B. Kirk, S. K. Liew, W. F. Reichert, C. A. Wang, H. K. Choi, J. N. Walpole, J. K. Butler, W. F. Ferguson, Jr., R. K. DeFreez, and M. Felisky, "Characteristics of coherent two-dimensional grating surface emitting diode laser arrays during CW operation," *IEEE J. Quantum Electron.*, vol. 27, no. 6, pp. 1594–1608, Jun. 1991.

[18] M. Kasraian and D. Botez, "Single-lobed far-field radiation pattern from surface-emitting complex-coupled distributed-feedback diode lasers," *Appl. Phys. Lett.*, vol. 67, pp. 2783–2785, Nov. 1995.

[19] M. Kasraian and D. Botez, "Metal-grating-outcoupled, surface-emitting distributed-feedback diode lasers," *Appl. Phys. Lett.*, vol. 69, pp. 2795–2797, Nov. 1996.

[20] J. Lopez, G. Witjaksono, and D. Botez, "Single-mode, single-lobe operation of surface-emitting, second-order distributed feedback lasers," *Appl. Phys. Lett.*, vol. 75, pp. 885–887, Aug. 1999.

[21] G. Witjaksono, S. Li, J. J. Lee, D. Botez, and W. K. Chan, "Single-lobe, surface-normal beam surface emission from second-order distributed feedback lasers with half-wave grating phase shift," *Appl. Phys. Lett.*, vol. 83, pp. 5365–5367, Dec. 2003.

[22] T. Masood, S. Patterson, N. V. Amarasinghe, S. McWilliams, D. Phan, D. Lee, Z. A. Hilali, X. Zhang, G. A. Evans, and J. K. Butler, "Single-frequency 1310-nm AlGaInAs-InP grating-outcoupled surface-emitting lasers," *IEEE Photon. Technol. Lett.*, vol. 16, no. 3, pp. 726–728, Mar. 2004.

[23] N. Finger, W. Schrenk, and E. Gornik, "Analysis of TM-polarized DFB laser structures with metal surface gratings," *IEEE J. Quantum Electron.*, vol. 36, no. 7, pp. 780–786, Jul. 2000.

[24] D. Hofstetter, J. Faist, M. Beck, and U. Oesterle, "Surface-emitting 10.1 μm quantum-cascade distributed feedback lasers," *Appl. Phys. Lett.*, vol. 75, pp. 3769–3771, Dec. 1999.

[25] W. Schrenk, N. Finger, S. Gianordoli, L. Hvozdara, G. Strasser, and E. Gornik, "Surface-emitting distributed feedback quantum-cascade lasers," *Appl. Phys. Lett.*, vol. 77, pp. 2086–2088, Oct. 2000.

[26] D. Hofstetter, J. Faist, M. Beck, A. Müller, and U. Oesterle, "Edge- and surface-emitting 10.1 μm quantum cascade distributed feedback lasers," *Physica E*, vol. 7, pp. 25–28, 2000.

[27] C. Pflügl, M. Austerer, W. Schrenk, S. Golka, G. Strasser, R. P. Green, L. R. Wilson, J. W. Cockburn, A. B. Krysa, and J. S. Roberts, "Single-mode surface-emitting quantum-cascade lasers," *Appl. Phys. Lett.*, vol. 86, pp. 211101-1–211101-3, May 2005.

[28] J. A. Fan, M. A. Belkin, and F. Capasso, "Surface emitting terahertz quantum cascade laser with a double-metal waveguide," *Opt. Exp.*, vol. 14, pp. 11672–11680, Nov. 2006.

[29] S. Kumar, B. S. Williams, Q. Qin, A. W. M. Lee, and Q. Hu, "Surface-emitting distributed feedback terahertz quantum-cascade lasers in metal–metal waveguides," *Opt. Exp.*, vol. 15, pp. 114–128, Jan. 2007.

[30] E. Mujagić, L. K. Hoffmann, S. Schartner, M. Nobile, W. Schrenk, M. P. Semtsiv, M. Wienold, W. T. Masselink, and G. Strasser, "Low divergence single-mode surface emitting quantum cascade ring lasers," *Appl. Phys. Lett.*, vol. 93, pp. 161101-1–161101-3, Oct. 2008.

[31] L. Mahler, A. Tredicucci, F. Beltram, C. Walther, J. Faist, B. Witzigmann, H. E. Beere, and D. A. Ritchie, "Vertically emitting microdisk lasers," *Nature Photon.*, vol. 3, pp. 46–49, Jan. 2009.

[32] O. Painter, R. K. Lee, A. Scherer, A. Yariv, J. D. O'Brien, P. D. Dapkus, and I. Kim, "Two-dimensional photonic band-gap defect mode laser," *Science*, vol. 284, pp. 1819–1821, Jun. 1999.

[33] R. Colombelli, K. Srinivasan, M. Troccoli, O. Painter, C. F. Gmachl, D. M. Tennant, A. M. Sergent, D. L. Sivco, A. Y. Cho, and F. Capasso, "Quantum cascade surface-emitting photonic crystal laser," *Science*, vol. 302, pp. 1374–1377, Nov. 2003.

[34] X. Letartre, C. Monat, C. Seassal, and P. Viktorovitch, "Analytical modeling and an experimental investigation of two-dimensional photonic crystal microlasers: Defect state (microcavity) versus band-edge state (distributed feedback) structures," *J. Opt. Soc. Amer. B*, vol. 22, pp. 2581–2595, Dec. 2005.

[35] E. Miyai, K. Sakai, T. Okano, W. Kunishi, D. Ohnishi, and S. Noda, "Lasers producing tailored beams," *Nature*, vol. 441, p. 946, Jun. 2006.

[36] H. Matsubara, S. Yoshimoto, H. Saito, Y. Jianglin, Y. Tanaka, and S. Noda, "GaN photonic-crystal surface-emitting laser at blue-violet wavelengths," *Science*, vol. 319, pp. 445–447, Jan. 2008.

[37] L. Sirigu, R. Terazzi, M. I. Amanti, M. Giovannini, J. Faist, L. A. Dunbar, and R. Houdré, "Terahertz quantum cascade lasers based on two-dimensional photonic crystal resonators," *Opt. Exp.*, vol. 16, pp. 5206–5217, Apr. 2008.

[38] E. Miyai, K. Sakai, T. Okano, W. Kunishi, D. Ohnishi, and S. Noda, "Linearly-polarized single-lobed beam in a surface-emitting photonic-crystal laser," *Appl. Phys. Exp.*, vol. 1, pp. 062002-1–062002-3, May 2008.

[39] Y. Chassagneux, R. Colombelli, W. Maineult, S. Barbieri, H. E. Beere, D. A. Ritchie, S. P. Khanna, E. H. Linfield, and A. G. Davies, "Electrically pumped photonic-crystal terahertz lasers controlled by boundary conditions," *Nature*, vol. 457, pp. 174–178, Jan. 2009.

[40] D. R. Scifres, R. D. Burnham, and W. Streifer, "Lateral grating array high power CW visible semiconductor laser," *Electron. Lett.*, vol. 18, no. 13, pp. 549–550, Jun. 1982.

[41] J. P. Hohimer, A. Owyoung, and G. R. Hadley, "Single-channel injection locking of a diode-laser array with a cw dye laser," *Appl. Phys. Lett.*, vol. 47, pp. 1244–1246, Dec. 1985.

[42] J. N. Baillargeon, P. K. York, C. A. Zmudzinski, G. E. Fernández, K. J. Beernink, and J. J. Coleman, "High-power phase-locked InGaAs strained-layer quantum well heterostructure periodic laser array," *Appl. Phys. Lett.*, vol. 53, pp. 457–459, Aug. 1988.

[43] Y. Ohno, D. K. Young, B. Beschoten, F. Matsukura, H. Ohno, and D. D. Awschalom, "Electrical spin injection in a ferromagnetic semiconductor heterostructure," *Nature*, vol. 402, pp. 790–792, Dec. 1999.

[44] R. Fiederling, P. Grabs, W. Ossau, G. Schmidt, and L. W. Molenkamp, "Detection of electrical spin injection by light-emitting diodes in top- and side-emission configurations," *Appl. Phys. Lett.*, vol. 82, pp. 2160–2162, Mar. 2003.

[45] M. Holub, J. Shin, S. Chakrabarti, and P. Bhattacharya, "Electrically injected spin-polarized vertical-cavity surface-emitting lasers," *Appl. Phys. Lett.*, vol. 87, pp. 091108-1–091108-3, Aug. 2005.

[46] D. Hägele and M. Oestreich, "Comment on 'Electrically injected spin-polarized vertical-cavity surface-emitting lasers' [Appl. Phys. Lett. 87, 091108-1-091108-3, 2005]," *Appl. Phys. Lett.*, vol. 88, pp. 056101–056101-1, Feb. 2006.

[47] H. A. Atwater, "The promise of plasmonics," *Sci. Amer.*, vol. 296, no. 4, pp. 56–63, Apr. 2007.

[48] E. Ozbay, "Plasmonics: Merging photonics and electronics at nanoscale dimensions," *Science*, vol. 311, pp. 189–193, Jan. 2006.

[49] D. R. Scifres, W. Streifer, and R. D. Burnham, "Beam scanning with twin-stripe injection lasers," *Appl. Phys. Lett.*, vol. 33, pp. 702–704, Oct. 1978.

[50] P. D. Henshaw, "Laser beamsteering using the photorefractive effect," *Appl. Opt.*, vol. 21, pp. 2323–2325, Jul. 1982.

[51] J. Katz, E. Kapon, C. Lindsey, S. Margalit, and A. Yariv, "Far-field distribution of semiconductor phase-locked arrays with multiple contacts," *Electron. Lett.*, vol. 19, no. 17, pp. 660–662, Aug. 1983.

[52] P. F. Mcmanamon, T. A. Dorschner, D. L. Corkum, L. J. Friedman, D. S. Hobbs, M. Holz, S. Liberman, H. Q. Nguyen, D. P. Resler, R. C. Sharp, and E. A. Watson, "Optical phased array technology," *Proc. IEEE*, vol. 84, no. 2, pp. 268–298, Feb. 1996.

[53] J. Durnin, J. J. Miceli, Jr., and J. H. Eberly, "Diffraction-free beams," *Phys. Rev. Lett.*, vol. 58, pp. 1499–1501, Apr. 1987.

[54] J. Durnin, "Exact solutions for nondiffracting beams. I. The scalar theory," *J. Opt. Soc. Amer. A*, vol. 4, pp. 651–654, Apr. 1987.

[55] V. S. Ilchenko, M. Mohageg, A. A. Savchenkov, A. B. Matsko, and L. Maleki, "Efficient generation of truncated Bessel beams using cylindrical waveguides," *Opt. Exp.*, vol. 15, pp. 5866–5871, Apr. 2007.

[56] T. Grosjean, D. Courjon, and D. V. Labeke, "Bessel beams as virtual tips for near-field optics," *J. Microsc.*, vol. 210, pp. 319–323, Jun. 2003.

[57] Z. Bomzon, V. Kleiner, and E. Hasman, "Formation of radially and azimuthally polarized light using space-variant subwavelength metal stripe gratings," *Appl. Phys. Lett.*, vol. 79, pp. 1587–1589, Sep. 2001.

[58] A. V. Nesterov, V. G. Niziev, and V. P. Yakunin, "Generation of high-power radially polarized beam," *J. Phys. D: Appl. Phys.*, vol. 32, pp. 2871–2875, Sep. 1999.

[59] R. Oron, S. Blit, N. Davidson, A. A. Friesem, Z. Bomzon, and E. Hasman, "The formation of laser beams with pure azimuthal or radial polarization," *Appl. Phys. Lett.*, vol. 77, pp. 3322–3324, Nov. 2000.

[60] S. C. Tidwell, G. H. Kim, and W. D. Kimura, "Efficient radially polarized laser beam generation with a double interferometer," *Appl. Opt.*, vol. 32, pp. 5222–5229, Sep. 1993.

[61] T. Grosjean, D. Courjon, and M. Spajer, "An all-fiber device for generating radially and other polarized light beams," *Opt. Commun.*, vol. 203, pp. 1–5, Mar. 2002.

[62] R. Beth, "Mechanical detection and measurement of the angular momentum of light," *Phys. Rev.*, vol. 50, pp. 115–125, Jul. 1936.

[63] M. Padgett, J. Courtial, and L. Allen, "Light's orbital angular momentum," *Phys. Today*, vol. 57, pp. 35–40, May 2004.

[64] L. Allen, M. W. Beijersbergen, R. J. C. Spreeuw, and J. P. Woerdman, "Orbital angular momentum of light and the transformation of Laguerre–Gaussian laser modes," *Phys. Rev. A*, vol. 45, pp. 8185–8189, Jun. 1992.

[65] M. W. Beijersbergen, L. Allen, H. E. L. O. Van Der Veen, and J. P. Woerdman, "Astigmatic laser mode converters and transfer of orbital angular momentum," *Opt. Commun.*, vol. 96, pp. 123–132, Feb. 1993.

[66] H. He, M. E. J. Friese, N. R. Heckenberg, and H. Rubinsztein-Dunlop, "Direct observation of transfer of angular momentum to absorptive particles from a laser beam with a phase singularity," *Phys. Rev. Lett.*, vol. 75, pp. 826–829, Jul. 1995.

[67] M. E. J. Friese, T. A. Nieminen, N. R. Heckenberg, and H. Rubinsztein-Dunlop, "Optical alignment and spinning of laser-trapped microscopic particles," *Nature*, vol. 394, pp. 348–350, Jul. 1998.

[68] E. Cubukcu, E. A. Kort, K. B. Crozier, and F. Capasso, "Plasmonic laser antenna," *Appl. Phys. Lett.*, vol. 89, pp. 093120-1–093120-3, Aug. 2006.

[69] N. Yu, E. Cubukcu, L. Diehl, M. A. Belkin, K. B. Crozier, F. Capasso, D. Bour, S. Corzine, and G. Höfler, "Plasmonic quantum cascade laser antenna," *Appl. Phys. Lett.*, vol. 91, pp. 173113-1–173113-3, Oct. 2007.

[70] N. Yu, E. Cubukcu, L. Diehl, D. Bour, S. Corzine, J. Zhu, G. Höfler, K. B. Crozier, and F. Capasso, "Bowtie plasmonic quantum cascade laser antenna," *Opt. Exp.*, vol. 15, pp. 13272–13281, Oct. 2007.

[71] T. Mukaihara, N. Ohnoki, Y. Hayashi, N. Hatori, F. Koyama, and K. Iga, "Polarization control of vertical-cavity surface-emitting lasers using a birefringent metal/dielectric polarizer loaded on top distributed Bragg reflector," *IEEE J. Sel. Topics Quantum Electron.*, vol. 1, no. 2, pp. 667–673, Jun. 1995.

[72] J.-H. Ser, Y.-G. Ju, J.-H. Shin, and Y. H. Lee, "Polarization stabilization of vertical-cavity top-surface-emitting lasers by inscription of fine metal-interlaced gratings," *Appl. Phys. Lett.*, vol. 66, pp. 2769–2771, May 1995.

[73] C.-A. Berseth, B. Dwir, I. Utke, H. Pier, A. Rudra, V. P. Iakovlev, E. Kapon, and M. Moser, "Vertical cavity surface emitting lasers incorporating structured mirrors patterned by electron-beam lithography," *J. Vac. Sci. Technol. B*, vol. 17, pp. 3222–3225, Nov./Dec. 1999.

[74] P. Debernardi, J. M. Ostermann, M. Feneberg, C. Jalics, and R. Michalzik, "Reliable polarization control of VCSELs through monolithically integrated surface gratings: A comparative theoretical and experimental study," *IEEE J. Sel. Topics Quantum Electron.*, vol. 11, no. 1, pp. 107–116, Jan./Feb. 2005.

[75] S. Boutami, B. Benbakir, J.-L. Leclercq, and P. Viktorovitch, "Compact and polarization controlled 1.55 μm vertical-cavity surface emitting laser using single-layer photonic crystal mirror," *Appl. Phys. Lett.*, vol. 91, pp. 071105-1–071105-3, Aug. 2007.

[76] P. B. Dayal and F. Koyama, "Polarization control of 0.85 μm vertical-cavity surface-emitting lasers integrated with gold nanorod arrays," *Appl. Phys. Lett.*, vol. 91, pp. 111107-1–111107-3, Sep. 2007.

[77] M. C. Y. Huang, Y. Zhou, and C. J. Chang-Hasnain, "A surface-emitting laser incorporating a high-index-contrast subwavelength grating," *Nature Photon.*, vol. 1, pp. 119–122, Feb. 2007.

[78] H. J. Lezec, A. Degiron, E. Devaux, R. A. Linke, L. Martin-Moreno, F. J. Garcia-Vidal, and T. W. Ebbesen, "Beaming light from a subwavelength aperture," *Science*, vol. 297, pp. 820–822, Aug. 2002.

[79] J. Gao, G. Song, Q. Gan, B. Guo, and L. Chen, "Surface plasmon modulated nano-aperture vertical-cavity surface-emitting laser," *Laser Phys. Lett.*, vol. 4, pp. 234–237, 2007.

[80] J. Feng, T. Okamoto, and S. Kawata, "Highly directional emission via coupled surface-plasmon tunneling from electroluminescence in organic light-emitting devices," *Appl. Phys. Lett.*, vol. 87, pp. 241109-1–241109-3, Dec. 2005.

[81] J. Feng and T. Okamoto, "Enhancement of electroluminescence through a two-dimensional corrugated metal film by grating-induced surface-plasmon cross coupling," *Opt. Lett.*, vol. 30, pp. 2302–2304, Sep. 2005.

[82] M. D. Harries and H. D. Summers, "Directional control of light-emitting-diode emission via a subwavelength-apertured metal surface," *IEEE Photon. Technol. Lett.*, vol. 18, no. 21, pp. 2197–2199, Nov. 2006.

[83] N. Yu, J. Fan, Q. J. Wang, C. Pflügl, L. Diehl, T. Edamura, M. Yamanishi, H. Kan, and F. Capasso, "Small-divergence semiconductor lasers by plasmonic collimation," *Nature Photon.*, vol. 2, pp. 564–570, Sep. 2008.

[84] N. Yu, R. Blanchard, J. Fan, T. Edamura, M. Yamanishi, H. Kan, and F. Capasso, "Small divergence semiconductor lasers with two-dimensional plasmonic collimators," *Appl. Phys. Lett.*, vol. 93, pp. 181101-1–181101-3, Nov. 2008.

[85] N. Yu, R. Blanchard, J. Fan, Q. J. Wang, C. Pflügl, L. Diehl, T. Edamura, M. Yamanishi, H. Kan, and F. Capasso, "Quantum cascade lasers with integrated plasmonic antenna-array collimators," *Opt. Exp.*, vol. 16, pp. 19447–19461, Nov. 2008.

[86] J. Faist, F. Capasso, D. L. Sivco, C. Sirtori, A. L. Hutchinson, and A. Y. Cho, "Quantum cascade laser," *Science*, vol. 264, pp. 553–556, Apr. 1994.

[87] L. Martín-Moreno, F. J. García-Vidal, H. J. Lezec, A. Degiron, and T. W. Ebbesen, "Theory of highly directional emission from a single subwavelength aperture surrounded by surface corrugations," *Phys. Rev. Lett.*, vol. 90, pp. 167401-1–167401-4, Apr. 2003.

[88] L.-B. Yu, D.-Z. Lin, Y.-C. Chen, Y.-C. Chang, K.-T. Huang, J.-W. Liaw, J.-T. Yeh, J.-M. Liu, C.-S. Yeh, and C.-K. Lee, "Physical origin of directional beaming emitted from a subwavelength slit," *Phys. Rev. B*, vol. 71, pp. 041405-1–041405-4, Jan. 2005.

[89] F. J. García-Vidal, L. Martín-Moreno, H. J. Lezec, and T. W. Ebbesen, "Focusing light with a single subwavelength aperture flanked by surface corrugations," *Appl. Phys. Lett.*, vol. 83, pp. 4500–4502, Dec. 2003.

[90] S. S. Akarca-Biyikli, I. Bulu, and E. Ozbay, "Enhanced transmission of microwave radiation in one-dimensional metallic gratings with subwavelength aperture," *Appl. Phys. Lett.*, vol. 85, pp. 1098–1100, Aug. 2004.

[91] H. Caglayan, I. Bulu, and E. Ozbay, "Beaming of electromagnetic waves emitted through a subwavelength annular aperture," *J. Opt. Soc. Amer. B*, vol. 23, pp. 419–422, Mar. 2006.

[92] C. Wang, C. Du, and X. Luo, "Refining the model of light diffraction from a subwavelength slit surrounded by grooves on a metallic film," *Phys. Rev. B*, vol. 74, pp. 245403-1–245403-7, Dec. 2006.

[93] D. Lin, T. Cheng, C. Chang, J. Yeh, J. Liu, C. Yeh, and C. Lee, "Directional light beaming control by a subwavelength asymmetric surface structure," *Opt. Exp.*, vol. 15, pp. 2585–2591, Mar. 2007.

[94] S. Kim, H. Kim, Y. Lim, and B. Lee, "Off-axis directional beaming of optical field diffracted by a single subwavelength metal slit with asymmetric dielectric surface gratings," *Appl. Phys. Lett.*, vol. 90, pp. 051113-1–051113-3, Feb. 2007.

[95] J. A. Kong, *Electromagnetic Wave Theory*. Cambridge, MA: EMW Publishing, 2000, ch. 4, pp. 526–551; ch. 4, p. 516.

[96] W. L. Stutzman and G. A. Thiele, *Antenna Theory and Design*. New York: Wiley, 1981, ch. 1, pp. 36–38.

[97] L. Novotny and B. Hecht, *Principles of Nano-Optics*. Cambridge, U.K.: Cambridge Univ. Press, 2006, ch. 12, p. 386.

[98] G. Lévêque, O. J. F. Martin, and J. Weiner, "Transient behavior of surface plasmon polaritons scattered at a subwavelength groove," *Phys. Rev. B*, vol. 76, pp. 155418-1–155418-8, Oct. 2007.

[99] G. Gay, O. Alloschery, B. V. de Lesegno, C. O'Dwyer, J. Weiner, and H. J. Lezec, "The optical response of nanostructured surfaces and the composite diffracted evanescent wave model," *Nature Phys.*, vol. 2, pp. 262–267, Apr. 2006.

[100] P. Lalanne and J. P. Hugonin, "Interaction between optical nano-objects at metallo-dielectric interfaces," *Nature Phys.*, vol. 2, pp. 551–556, Aug. 2006.

[101] W. L. Barnes, T. W. Preist, S. C. Kitson, and J. R. Sambles, "Physical origin of photonic energy gaps in the propagation of surface plasmons on gratings," *Phys. Rev. B*, vol. 54, pp. 6227–6244, Sep. 1996.

[102] A. Taflove and S. C. Hagness, *Computational Electrodynamics: The Finite-Difference Time-Domain Method*, 2nd ed. Norwood, MA: Artech House, 2000, ch. 8, pp. 349–372.

[103] E. D. Palik, *Handbook of Optical Constants of Solids*. Orlando, FL: Academic, 1985, pp. 286–295.

[104] E. D. Palik, *Handbook of Optical Constants of Solids II*. San Diego, CA: Academic, 1991, pp. 761–776.

[105] N. Yu, M. A. Kats, C. Pflügl, M. Geiser, Q. J. Wang, M. A. Belkin, F. Capasso, M. Fischer, A. Wittmann, J. Faist, T. Edamura, S. Furuta, M. Yamanishi, and H. Kan, "Multi-beam multi-wavelength semiconductor lasers," *Appl. Phys. Lett.*, vol. 95, pp. 161108-1–161108-3, Oct. 2009.

[106] S.-H. Chang, S. Gray, and G. Schatz, "Surface plasmon generation and light transmission by isolated nanoholes and arrays of nanoholes in thin metal films," *Opt. Exp.*, vol. 13, pp. 3150–3165, Apr. 2005.

[107] L. Yin, V. K. Vlasko-Vlasov, A. Rydh, J. Pearson, U. Welp, S.-H. Chang, S. K. Gray, G. C. Schatz, D. B. Brown, and C. W. Kimball, "Surface plasmons at single nanoholes in Au films," *Appl. Phys. Lett.*, vol. 85, pp. 467–469, Jul. 2004.

[108] J. M. Steele, Z. Liu, Y. Wang, and X. Zhang, "Resonant and non-resonant generation and focusing of surface plasmons with circular gratings," *Opt. Exp.*, vol. 14, pp. 5664–5670, Jun. 2006.

[109] K. Fujita, S. Furuta, A. Sugiyama, T. Ochiai, T. Edamura, N. Akikusa, M. Yamanishi, and H. Kan, "Room temperature, continuous-wave operation of quantum cascade lasers with single phonon resonance-continuum depopulation structures grown by metal organic vapor-phase epitaxy," *Appl. Phys. Lett.*, vol. 91, pp. 141121-1–141121-3, Oct. 2007.

[110] X. Shi, L. Hesselink, and R. Thornton, "Ultrahigh light transmission through a C-shaped nanoaperture," *Opt. Lett.*, vol. 28, pp. 1320–1322, Aug. 2003.

[111] F. Chen, A. Itagi, J. A. Bain, D. D. Stancil, T. E. Schlesinger, L. Stebounova, G. C. Walker, and B. B. Akhremitchev, "Imaging of optical field confinement in ridge waveguides fabricated on very-small-aperture laser," *Appl. Phys. Lett.*, vol. 83, pp. 3245–3247, Oct. 2003.

[112] X. Shi and L. Hesselink, "Design of a C aperture to achieve λ/10 resolution and resonant transmission," *J. Opt. Soc. Amer. B*, vol. 21, pp. 1305–1317, Jul. 2004.

[113] J. A. Matteo, D. P. Fromm, Y. Yuen, P. J. Schuck, W. E. Moerner, and L. Hesselink, "Spectral analysis of strongly enhanced visible light transmission through single C-shaped nanoapertures," *Appl. Phys. Lett.*, vol. 85, pp. 648–650, Jul. 2004.

[114] Z. Rao, J. A. Matteo, L. Hesselink, and J. S. Harris, "High-intensity C-shaped nanoaperture vertical-cavity surface-emitting laser with controlled polarization," *Appl. Phys. Lett.*, vol. 90, pp. 191110-1–191110-3, May 2007.

[115] H. Gai, J. Wang, Q. Tian, W. Xia, and X. Xu, "Matching the emitting wavelength from a very-small-aperture laser to the resonant property of a nanometric C-aperture," *Appl. Opt.*, vol. 46, pp. 7746–7750, Nov. 2007.

[116] K. Tanaka and M. Tanaka, "Simulation of confined and enhanced optical near-fields for an I-shaped aperture in a pyramidal structure on a thick metallic screen," *J. Appl. Phys.*, vol. 95, pp. 3765–3771, Apr. 2004.

[117] K. Tanaka, M. Tanaka, and T. Sugiyama, "Metallic tip probe providing high intensity and small spot size with a small background light in near-field optics," *Appl. Phys. Lett.*, vol. 87, pp. 151116-1–151116-3, Oct. 2005.

[118] R. Azadegan and K. Sarabandi, "A novel approach for miniaturization of slot antennas," *IEEE Trans. Antennas Propag.*, vol. 51, no. 3, pp. 421–429, Mar. 2003.

[119] S. Y. Chou, P. R. Krauss, and P. J. Renstrom, "Imprint lithography with 25-nanometer resolution," *Science*, vol. 272, pp. 85–87, Apr. 1996.

[120] P. C. Hidber, W. Helbig, E. Kim, and G. M. Whitesides, "Microcontact printing of palladium colloids: Micron-scale patterning by electroless deposition of copper," *Langmuir*, vol. 12, pp. 1375–1380, Feb. 1996.

Nanfang Yu (M'06) received the B.S. degree in electronic information science and technology from the Department of Electronics, Peking University, Beijing, China, in 2004, and the Ph.D. degree in engineering sciences from Harvard University, Cambridge, MA, in June 2009.

Currently, he is a postdoctoral researcher in the School of Engineering and Applied Sciences at Harvard University, Cambridge, MA. His research interests include nanophotonics (e.g., plasmonics, metamaterials) and quantum cascade lasers.

Dr. Yu was a recipient of Chinese Government Award for Outstanding Self-financed Students Abroad in 2007. He is a student member of the Optical Society of America, the American Physical Society, and the Materials Research Society.

Romain Blanchard (S'08) was born in France in 1985. He received the M.Sc. degree from the Ecole Polytechnique, Palaiseau, France, in 2008. He is currently working toward the Ph.D. degree at the School of Engineering and Applied Sciences, Harvard University, Cambridge, MA.

His current research interests include mid-IR plasmonics and photonic crystals.

Mr. Blanchard was awarded the Research Internship Grand Prix in physics of the Ecole Polytechnique for his work on plasmonic collimation during the summer of 2008.

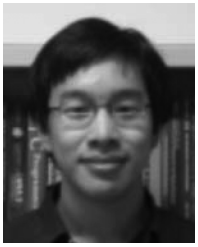

Jonathan Fan received the B.S.E. degree in electrical engineering and a certificate in engineering physics from Princeton University, Princeton, NJ. He is currently working toward the Ph.D. degree at the School of Engineering and Applied Sciences, Harvard University, Cambridge, MA.

His current research interests include terahertz and mid-IR quantum cascade lasers, functional plasmonics, and metamaterials.

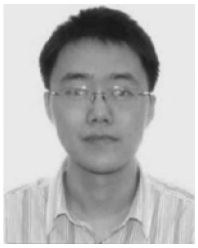

Qi Jie Wang was born in Liaoning, China, in 1979. He received the B.E. degree in electrical engineering from the University of Science and Technology of China, Hefei, China, in 2001, and the Ph.D. degree in electrical and electronic engineering from Nanyang Technological University, Singapore, in 2005.

During 2005, he was a Singapore Millennium Foundation Fellow. He is currently with the School of Engineering and Applied Science, Harvard University, Cambridge, MA, where he was a Postdoctoral Researcher in January 2007. He has authored or coauthored more than 30 journal papers and numerous conference presentations. His current research interests include mid-IR and terahertz quantum cascade lasers, fiber optics and photonics, optical communications, and systems and signal processing.

Dr. Wang was a recipient of the Top Prize for the Young Inventor Awards of the International Society for Optical Engineers Photonics Europe Innovation Village in 2004, the Golden Award from the Fifth Young Inventor's Awards in 2005, and the Illuminating Engineering Society Prestigious Engineering Achievement Award 2005 of Singapore.

Christian Pflügl received the Diploma in physics from the University of Regensburg, Regensburg, Germany, in 2001, and the Ph.D. degree in electrical engineering from Vienna University of Technology, Vienna, Austria, in 2005.

From 2005 to 2006, he was a Postdoctoral Researcher at Vienna University of Technology, where he was involved in research on quantum cascade lasers. In 2006, he joined Harvard University, Cambridge, MA. His current research interests include high-performance and single-mode quantum cascade lasers as well as the physics of these devices, nonlinear optics, mid-IR plasmonics, microfabrication, and nanotechnology.

Laurent Diehl was born in Switzerland in 1976. He received the Ph.D. degree from the University of Neuchâtel, Neuchâtel, Switzerland, in 2003.

In 2003, he joined Harvard University, Cambridge, MA, as a Postdoctoral Fellow, where he later became a Research Associate. He is currently involved in the development of high-power quantum cascade lasers grown by metal–organic chemical vapor deposition, as well as the physics of these devices, including their ultrafast dynamics. His current research interests include the development of p-type Si/SiGe quantum cascade lasers.

Dr. Diehl was a corecipient of the Swiss Physical Society's IBM award in 2001.

Tadataka Edamura was born in Tokyo, Japan, in 1967. He received the B.S., M.S., and Ph.D. degrees in applied physics from Keio University, Yokohama, Japan, in 1990, 1992, and 1995, respectively.

In April 1995, he joined Hamamatsu Photonics K.K., Hamamatsu, Japan, where he is currently an Associate Senior Researcher in the Central Research Laboratory. He has been involved in the research and development of mid-IR semiconductor devices, especially quantum cascade lasers as well as crystal growth by the molecular beam epitaxy technique.

Dr. Edamura is a member of the Japan Society of Applied Physics.

Shinichi Furuta was born in Shizuoka, Japan, in 1969. He received the M.S. degree in material engineering from Nagoya University, Aichi, Japan, in 1994.

In April 1994, he joined Hamamatsu Photonics K.K., Hamamatsu, Japan, where he is involved in the research and development of quantum cascade lasers, primarily concerning with crystal growth by metal–organic vapor phase epitaxy technique for the device uses.

Mr. Furuta is a member of the Japan Society of Applied Physics.

Masamichi Yamanishi (M'72–SM'92–F'97–LF'07) received the B.S., M.S., and Ph.D. degrees in electrical engineering from the University of Osaka Prefecture, Sakai, Japan, in 1964, 1966, and 1971, respectively.

In 1966, he joined the Department of Electrical Engineering, University of Osaka Prefecture, as a Research Associate. In 1979, he was appointed as an Associate Professor in the Department of Physical Electronics, Hiroshima University, Hiroshima, Japan, where he was promoted to a Full Professor in 1983, was the Dean of the newly established Graduate School of Advanced Sciences of Matter from 1998 to 2001, the Vice President during 2001–2003, and is currently a Professor Emeritus. In 1984, 1986, 1987, and 1991, he was a Visiting Professor (Sabbatical Chair) at Purdue University, West Lafayette, IN. Since 2004, he has been a Technical Adviser with the Central Research Laboratory, Hamamatsu Photonics K.K., Hamamatsu, Japan. His current research interests include experimental and theoretical research on surface-acoustic-wave devices such as acoustic distributed-feedback (DFB) lasers, 2-D DFB lasers, theory of optical polarization dependence of interband transitions in semiconductor quantum-well (QW) structures, theory of gain spectra of semiconductor lasers based on non-Markovian relaxation dynamics, linear and ultrafast nonlinear (due to virtual excitons named VCON) electrooptic effects of semiconductor QW structures, their applications to high-speed field-effect semiconductor optical devices, including the first demonstration of field-effect light emitters proposed by himself, quantum manipulation of spontaneous emissions in semiconductor microcavities, terahertz electromagnetic wave generation by polarized-exciton-polaritons in microcavities, and photon number squeezing in semiconductor LEDs. He is the author of three book chapters on physics and applications of QW structures and a Co-Editor of an issue of *Selected Papers in Physics* on "Quantum manipulation of radiation field and matter" (Physical Society of Japan, 1997). He was a Far-East Editor of *Progress in Quantum Electronics* from 1996 to 1998. He has authored or coauthored more than 150 refereed papers published in scientific and technical journals, and has given more than 100 contributed talks and 41 invited talks, both at major international conferences. His current research interests include semiconductor lasers including quantum cascade lasers.

Prof. Yamanishi is a Fellow of the Japan Society of Applied Physics, a member of the Physical Society of Japan and the Laser Society of Japan, and an Editorial Advisory Board Member of the Laser Focus World, Japan. He cochaired the Optical Society of America Topical Meetings on Quantum Wells for Optics and Optoelectronics (1989) and Quantum Optoelectronics (1991), both at Salt Lake City, UT. He was a recipient of the Achievement Award of Optics and Quantum Electronics of the Japan Society of Applied Physics in 2001 and the 60th Cultural Award of Cyuugoku Shinbunsya (a News Paper Company in Hiroshima) in 2003.

Hirofumi Kan received the B.S. and M.S. degrees in electrical engineering from Shizuoka University, Hamamatsu, Japan, in 1966 and 1968, respectively, and the Ph.D. degree in engineering from Tohoku University, Sendai, Japan, in 1982.

In 1968, he joined Mitsubishi Electric Corporation, where he was engaged in the research and development of continuous-wave laser diodes. In 1977, he joined Hamamtsu Photonics K.K., Hamamatsu, Japan, where he has been the Manager of the Material Research Section, Central Research Laboratory, since 1992, the Director since 1999, and has been involved in the research and development of high-power laser diodes. During 1977–1980, he was a Visiting Researcher at the Research Institute of Electronics, Shizuoka University, Hamamatsu, Japan, where, from 1992 to 1998, he was involved in the Yamamoto-Exploratory Research for Advanced Technology project on quantum fluctuations as a Research Member. His current research interests include high-power industrial lasers, short-pulse lasers, quantum cascade lasers, UV semiconductor lasers, specific light emitters and detectors, and crystal growth for device uses.

Dr. Kan is a member of the Japan Society of Applied Physics, the Laser Society of Japan, the Institute of Electronics, Information and Communication Engineers, and the Institute of Electrical Engineers of Japan.

Federico Capasso (M'79–SM'85–F'87) received the Dr. Phys. degree (*summa cum laude*) from the University of Rome, Rome, Italy, in 1973.

From 1974 to 1976, he was a Researcher at Fondazione Ugo Bordoni. In 1976, he joined Bell Laboratories, where he was a Member of the Technical Staff (1977–1986), the Department Head (1986–2000), the Vice President for Physical Research (2000–2002), and was made a Bell Laboratories Fellow for his scientific contributions in 1997. He is currently the Robert Wallace Professor of Applied Physics and Vinton Hayes Senior Research Fellow in Electrical Engineering at Harvard University, Cambridge, MA. He has been engaged in basic and applied research on the quantum design of new artificial materials and devices, known as band structure engineering, and also in investigations of the Casimir effect and the field of surface plasmon photonics. He is a co-inventor of the quantum cascade laser. More recently, he initiated a new line of research using microelectromechanical systems to investigate the basic physics of Casimir effect and its applications to nanomechanics. He has authored or coauthored more than 300 papers, edited four volumes, and holds more than 40 U.S. patents.

Prof. Capasso is a member of the National Academy of Sciences, the National Academy of Engineering, and the American Academy of Arts and Sciences. His awards include the King Faisal International Prize for Science, the IEEE Edison Medal, the Arthur Schawlow Prize in Laser Science, the Wetherill Medal of the Franklin Institute, the RobertWood Prize of the Optical Society of America (OSA), the William Streifer Award of the Laser and Electro-Optic Society (IEEE), the Rank Prize in Optoelectronics (U.K.), the IEEE David Sarnoff Award in Electronics, the Duddell Medal of the Institute of Physics (U.K.), the Willis Lamb Medal for Laser Science and Quantum Optics, the Materials Research Society Medal, the "Vinci of Excellence" Prize (France), the Welker Memorial Medal (Germany), the New York Academy of Sciences Award, and the Newcomb Cleveland Prize of the American Association for the Advancement of Science. He is a Fellow of the OSA, the American Physical Society, the International Society for Optical Engineering, and the American Association for the Advancement of Science.